4

Lab-on-a-Chip Devices with Organic Semiconductor-Based Optical Detection

O. Hofmann, D.D.C. Bradley, J.C. deMello, and A.J. deMello

4.1 Introduction

4.1.1 Microfluidics and Lab-on-a-Chip

On 29 December 1959, the Nobel Laureate Richard Feynman delivered his prophetic talk before the American Physical Society in which he contemplated the potentials of miniaturization in the physical sciences. His vision, based on known technology, scrutinized the limits set by physical principles and suggested a range of new "nano-tools," including the concept of "atom-by-atom" fabrication. As we now know, over the intervening decades, many of these predictions have become reality. For example, microelectronic circuits have shrunk to sizes that approach the molecular level, scanning probe microscopes can image and manipulate individual atoms, and the molecular machinery of living systems is now being more fully understood and harnessed.

It is therefore surprising that it is only within the last 20 years that the concepts of miniaturization have been seriously applied to the fields of chemical and biological analysis. Of particular interest has been the development and application of microfluidic or *lab-on-a-chip* technology. In simple terms, microfluidics describes the study and development of systems that manipulate and process small instantaneous amounts of fluid (typically on the picoliter to nanoliter scale) using features whose characteristic dimensions are most conveniently measured in microns. Interest in such technology has been driven by a range of fundamental features that accompany system miniaturization. Such features include the ability to process and handle small volumes of fluid, improved analytical performance when compared to their macroscale analogues, reduced instrumental footprints, low unit cost, facile integration of functional components, and the exploitation of atypical fluid dynamics to control molecules in both time and space [1]. Based on these advantageous characteristics, microfluidic chip devices (such as those shown in Figs. 4.1–4.4) have been used to good effect in a wide variety of applications, including nucleic acid separations, protein analysis, process control, small-molecule

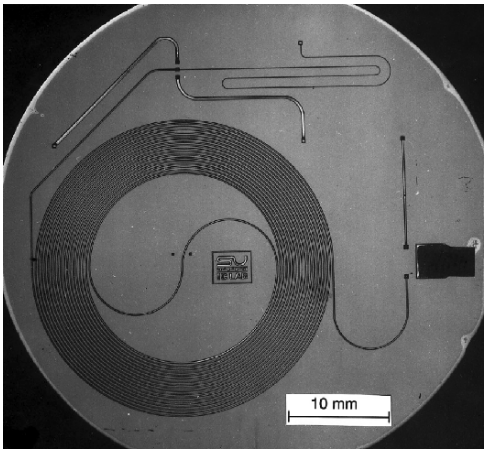

Fig. 4.1. Lab-on-a-chip gas chromatograph on silicon substrate (From [4] – Copyright 1979 IEEE)

organic synthesis, DNA amplification, immunoassays, DNA sequencing, cell manipulations, nanomaterial synthesis, and medical diagnostics [2, 3].

Much of the early pioneering work centered on the transfer of established analytical methods from conventional (macroscale) to microfluidic (chip-based) formats. Specifically, a primary focus of these early studies was the creation of chip-based devices for performing analytical separations (based on chromatographic and electrophoretic phenomena). For example, it is generally recognized that the first lab-on-a-chip system, a gas chromatograph, was presented by Terry and coworkers in 1979 (Fig. 4.1) [4]. Structured on a 2-in. silicon wafer, the device integrated a spiral separation column, carrier-gas and sample injectors, and a thermal conductivity detector. In 1992, Manz and Harrison reported the first chip-based electrophoretic separations [5]. These and the subsequent studies marked an explosion in both academic and industrial interest in the field, due to the fact that by miniaturizing column dimensions and creating monolithic fluidic networks on planar substrates, huge enhancements in analytical performance in terms of analytical speed, component resolution, reproducibility, and analytical throughput could be achieved. Indeed, a survey of the current literature demonstrates that almost all separation methods (based on electrophoretic or chromatographic partitioning) have been successfully transferred to micromachined formats with enhanced performance characteristics. Such techniques include liquid chromatography, micellar electrokinetic capillary chromatography, synchronized cyclic capillary electrophoresis, free flow electrophoresis, and open channel electrochromatography.

A subsequent theme of much effort in the microfluidics community has been the development of integrated microfluidic systems. In conceptual form, the success of a microfluidic system is defined by its ability to rapidly and

efficiently extract required information from a chemical or biological system. This almost always involves performing a series of systematic operations on an analytical sample, which includes sample and reagent introduction, fluid motivation, reagent mixing and reaction, sample separation and purification, analyte detection, and product isolation. Indeed, one of the principal advantages of using microfabrication methods to create analytical instruments is the ease with which large-scale integration of functional components can be achieved. In recent years some elegant examples of functional integration of components have begun to revolutionize the way in which microfluidic tools are developed and used to solve fundamental problems. A good example has been the introduction of soft lithography in poly(dimethylsiloxane) as a fast and efficient route to microfluidic device manufacture. The elastomeric nature of this material has facilitated the development of sophisticated valve technologies (based on the restriction of fluidic channels via pneumatic actuation), which in turn have enabled the creation of highly integrated microfluidic circuits that can perform complex biological and chemical assays. An example of such an integrated system can be seen in Fig. 4.2. However, it should be realized that more traditional micromachining methods and materials (such as glass and silicon) can still be used to create microfluidic systems with high levels of integration and operational excellence. A good example, shown in Fig. 4.3, is a nanoliter-scale microfabricated bioprocessor that integrates thermal cycling, sample purification, and capillary electrophoresis for Sanger DNA sequencing [6].

Since microfluidic systems can rapidly manipulate, process, and analyze small volumes of complex fluids with high efficiency, their use as basic tools in medical and clinical diagnostics is an attractive prospect [7]. At the current time, a wide diversity of diseases such as infectious or cardiac diseases are

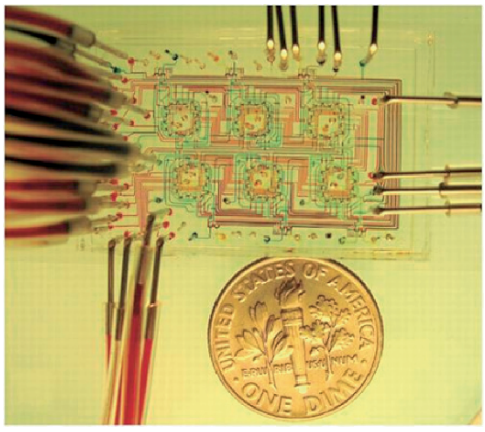

Fig. 4.2. Complex microfluidic circuit on polydimethylsiloxane (PDMS) substrate

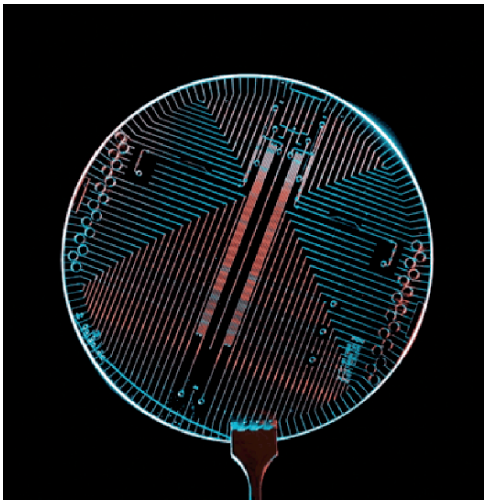

Fig. 4.3. Microfabricated bioprocessor for integrated DNA sequencing (From [6] – Copyright 2006 National Academy of Sciences, U.S.A.)

diagnosed using immunoassay methods. In simple terms, an immunoassay is a biochemical test that quantitatively measures the presence of a specific analyte in a biological fluid (typically serum, urine, or saliva) using the specific reaction of an antibody to its antigen. In the developed world, basic blood chemistry panels that integrate 10–20 separate tests of this kind are typically analyzed using automated, benchtop instruments located in centralized laboratories. Patient samples (e.g., 5 mL of whole blood) are normally collected at a hospital or physician's office and then transferred via a logistics chain to the centralized laboratory for testing. After a period of between 24 and 96 h, results are electronically returned to the physician who can then make a therapeutic decision and initiate treatment at a follow-up visit. For many tests, the time-to-result is not a critical factor; however, in cases where the patient may be experiencing, for example, acute cardiovascular disease, myocardial infarction, or a thromboembolic event, such large time delays are unacceptable. According to the American Heart Association, 64 million individuals in the US currently have acute cardiovascular disease, with over eight million emergency department admissions being associated with chest pains (and thus requiring rapid diagnosis of arrhythmia or myocardial infarction). Accordingly, the need for rapid and accurate diagnosis at the initial *point-of-care* is compelling (Fig. 4.4). This combined with a trend towards monitoring and control of long-term disease in home environments necessitates the development of diagnostic technologies that are cheap, fast, require minimal operator input, and provide unambiguous results.

Although significant advancements continue in public healthcare within the developed world, more than one billion people still lack the most basic

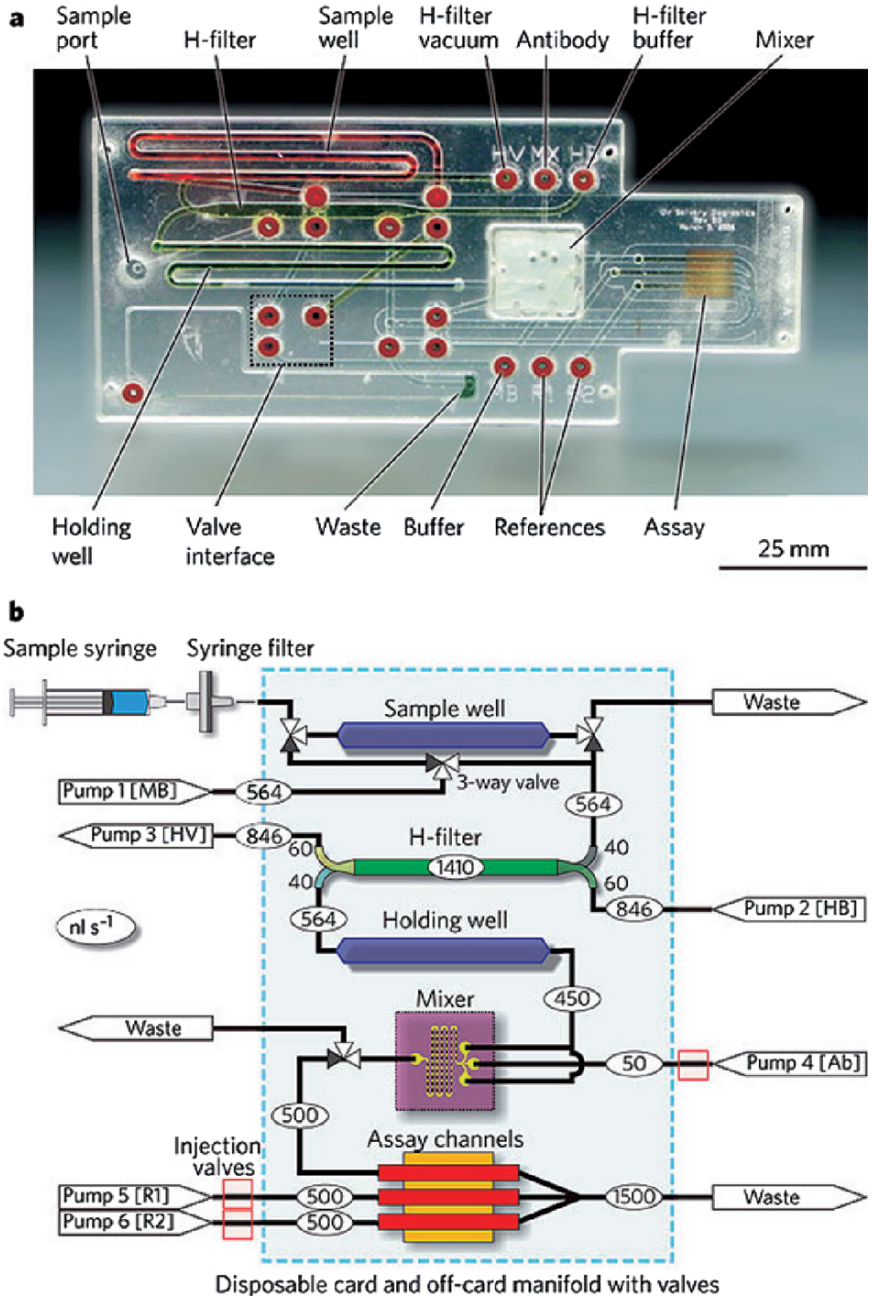

Fig. 4.4. Diagnostic test based on microfluidic lab-on-a-chip technology (From [7] – Copyright 2006 Nature Publishing Group)

healthcare facilities within developing and third world countries. As noted by Yager and coworkers, accomplishments such as the eradication of smallpox in 1979 have unfortunately been accompanied by the reemergence of infectious diseases such as tuberculosis and the appearance of new diseases such as HIV/AIDS. Since more than 50% of all deaths in the world's poorest regions are a result of infectious disease, the availability of appropriate diagnostic technologies could have a profound impact on healthcare in the twenty-first century. Nevertheless, the successful and widespread implementation of *point-of-care* diagnostic devices in a developing country is a nontrivial challenge. Not only must the devices be accurate, inexpensive, robust, and reliable, but they are likely to be used in settings that can be hot, humid, dirty, dusty, and lack electricity or running water. These complications are further exacerbated by the likelihood that the tests will be performed by partially trained or even untrained individuals.

As has been shown in numerous studies, microfluidic systems, on paper at least, may provide an ideal format for *point-of-care* diagnostics. They are able to process and manipulate small amounts of sample, can be mass-fabricated at low unit cost, can be operated by untrained personnel, and are able to operate in resource-poor environments. In recent years, a number of prototype microfluidic diagnostic devices have been reported. These developments have been reviewed in detail by Yager and coworkers, who conclude that the primary challenge associated with the successful deployment of microfluidic diagnostic systems relates to reducing unit costs to a level that is competitive with current lateral flow immunoassays (which although suitable for crude on-the-spot diagnosis must generally be followed by more quantitative testing at remote or centralized laboratories). A key factor in achieving this goal within the *point-of-care* diagnostic sector is the ability to perform sensitive analyte detection at low cost and in an integrated format.

4.1.2 Detection Problem at the Microscale

Clearly the use of microfluidic systems in chemical and biological analysis engenders considerable advantages with respect to performance markers such as speed, throughput, analytical performance, selectivity, automation, and control. All such gains are made possible by system downscaling and the associated improvements in mass and thermal transfer. Nonetheless, handling and processing fluidic samples with instantaneous volumes ranging from a few picoliters to hundreds of nanoliters represents a nontrivial challenge for analyte detection, and arguably defines the principle limitation of a microfluidic system in a specific application. In other words, although a reduction in scale may afford a significant improvement in analytical performance, this benefit is offset by a progressive decrease in the number of molecules available for detection. This issue is highlighted by a simple calculation: when performing capillary electrophoresis within a chip-based microfluidic system, analyte injection volumes are commonly no larger than 50 pL. This means that for

an analyte concentration of 10^{-9} mol L^{-1}, only about 30,000 molecules are present in the system for separation and detection!

Small volume detection within microfluidic environments has typically been based around optical measurements. Optical detection is well suited for most microfluidic systems due to the favorable optical characteristics of most substrate materials (including glasses, quartz, and plastics) in the visible region of the electromagnetic spectrum. Emission based optical techniques are usually the most sensitive, in particular, fluorescence- and chemiluminescence-based detection, in which analytes emit light in response to optical or chemical excitation, respectively. The most common chip-based detection methods include laser-induced fluorescence (LIF), UV–vis absorbance, chemiluminescence, refractive index variation, and thermal lens microscopy. Although attractive for the detection of small molecules, absorbance measurements are compromised due to the difficulty of probing small sample volumes while maintaining a sufficiently long optical pathlength to achieve appreciable absorption. By far, the most popular optical detection technique for chip-based analysis is LIF, which affords exceptional sensitivity and low mass detection limits at the expense of relatively sophisticated equipment.

As few as 10^5 molecules are routinely detected using LIF, and recent developments in ultra-high sensitivity fluorescence detection have allowed single molecule detection to be performed within microchannel environments [8]. A detailed evaluation of detection methods used for small-volume environments is provided elsewhere [9, 10]; however, it is important to appreciate that effective detection within microfluidic environments is clearly defined by a close interrelationship of factors such as detector sensitivity, optical coupling efficiencies, response times, detection limits, and information content.

The specific needs of *point-of-care* diagnostic devices in relation to analyte detection are unmistakable. Small sample volumes and low analyte concentrations typical in microfluidic systems make high sensitivity detection a prerequisite. While in the laboratory these demands may be met by sophisticated detection schemes using benchtop optical components such as lasers, photomultiplier tubes (PMTs), or fluorescence microscopes, the realization of portable diagnostic devices for *point-of-care* testing necessitates the development of integrated, inexpensive, versatile, and miniaturized detection modules. To date, few if any diagnostic systems with fully integrated, low-cost, and versatile optical detectors have been reported.

4.2 Fabrication

4.2.1 Microfluidic Systems

A cursory glance through microfluidic literature in the early 1990s reveals that almost all early microfluidic systems were constructed from glass, quartz, or silicon. This is unsurprising since standard photolithography and wet-etching

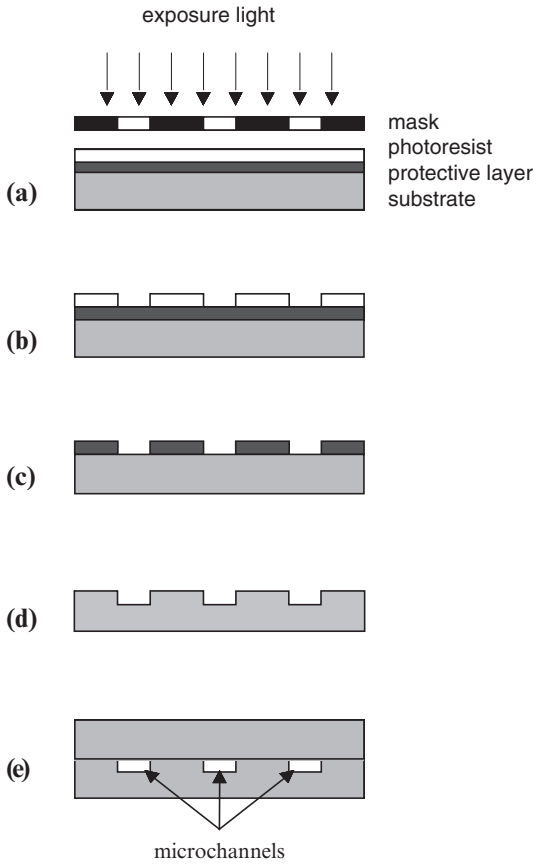

Fig. 4.5. Microfabrication process. (**a**) Photolithographic photoresist patterning. (**b**) Photoresist development. (**c**) Protective layer etching. (**d**) Substrate etching. (**e**) Bonding to cover plate

techniques perfected in the microelectronics and semiconductor industries could be used to efficiently structure all these materials to produce microchannel networks [11].

The generic microfabrication process used can be separated into three major stages; patterning, etching, and closure (Fig. 4.5). For silicon substrates a protective layer of silicon oxide is thermally grown at 200°C prior to processing. For photolithographic patterning, a positive photoresist is then spun onto the protective layer (Fig. 4.5a). UV exposure of the photoresist through a mask (defining the desired channel pattern) results in locally increased photoresist solubility. After dissolving such exposed regions of the photoresist (Fig. 4.5b), the uncovered silicon oxide can be etched (Fig. 4.5c). Depending on the required channel geometry, wet or dry etching techniques are applied to structure the underlying substrate (Fig. 4.5d). Etching silicon with a mixture

of hydrofluoric and nitric acid results in semicircular channels due to a nondirectional (or isotropic) etching action. For basic etchants such as potassium hydroxide the shape of the resulting channels depends on the crystallographic orientation of the silicon substrate. If etching occurs along the crystallographic planes, pyramidal pits or V-shaped grooves are obtained depending on the size of the etched area and the etching time. Dry etching techniques are based on the formation of reactive ion species in the gas phase. With guided ion beams, near-vertical side walls and high aspect ratios can be achieved at the expense of high instrumental costs and low etching rates.

After etching, the remaining protective layer and photoresist is removed and a second unstructured silicon wafer is bonded on top to enclose fluidic channels (Fig. 4.5e). Thermal fusion bonding above 600°C is based on the temperature-induced softening of the silicon–silicon interface and rehardening upon cooling. Anodic bonding can also be employed to bond a glass cover plate to the structured silicon substrate (Fig. 4.6). This process requires the application of a voltage of 700–1,200 V between the substrates (with silicon serving as the anode) and temperatures between 300 and 400°C. While micromachining techniques for silicon are well-established, there remain drawbacks with its use as a substrate material in microfluidic applications. For example, the low breakdown-voltage of silicon necessitates the growth of insulating layers (e.g., thermally grown silicon oxide) for electrophoretic applications. Furthermore, silicon is opaque in the visible wavelength range employed for most optical detection schemes.

In basic terms, glass microfabrication is identical to silicon microfabrication. Glass substrates are commonly coated with chromium to serve as the protective layer for etching. Wet etching techniques are almost always used for substrate structuring, with typical etching solutions comprising hydrofluoric acid and ammonium fluoride. Since glass has a noncrystalline structure, etching is isotropic, which limits the aspect ratios obtainable. The most common

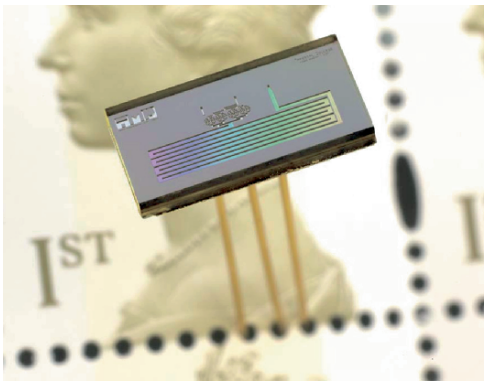

Fig. 4.6. Typical glass–silicon microfluidic device for diffusive mixing of two components

bonding technique for enclosing glass structures is thermal bonding, which requires application of temperatures of 600°C over several hours. However, recently alternative low temperature methods have been developed. These are based on the formation of an additional bonding layer, such as epoxy, sodium silicate, or a thin layer of HF between the glass surfaces resulting in temporary dissolution of the glass boundaries and subsequent rehardening. Glass microfluidic devices offer adequate electrical insulation and are optically transparent in the visible range, rendering them amenable for a much wider range of *lab-on-a-chip* applications compared to silicon. However, a limitation that silicon and glass microfabrication techniques have in common is that they are based on batch processing, i.e., only one substrate is processed at a time.

As previously discussed, a recent trend in microfluidic device fabrication is the use of polymers and elastomers that are amenable to replication technologies and allow for high-throughput and low-cost manufacture [12]. Photoablation is a method used to produce channels in a variety of polymeric substrates by means of "microexplosions" induced by pulsed UV-laser light. Hot Embossing is a common technique for imprinting micron-sized features on polymer substrates using a master mold (Fig. 4.7). Microfabricated Ni-shims are typically used for printing a layout in a thin polymer film, which is heated up to its softening point. This simple technique enables the fabrication of microstructures with high structural accuracy at low cost. Currently, the most advanced replication technology is injection molding. It enables the fabrication of very deep, high-quality microstructures in thick thermoplastic substrates. Because of the need for a high-pressure injection chamber into which the microfabricated Ni-shim is fixed, costs are slightly higher than for hot embossing. The described polymer micromachining methods typically offer straightforward bonding techniques. Taking advantage of the strongly temperature-dependent properties of most polymers, thermal

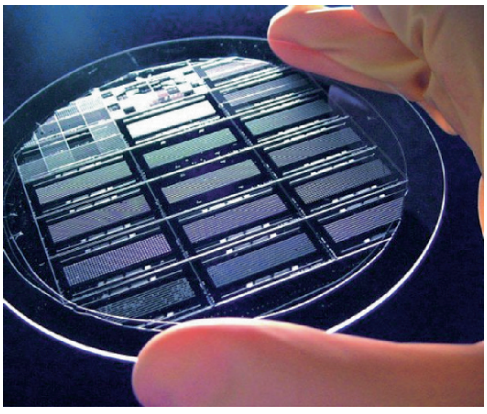

Fig. 4.7. Plastic microchip fabricated by hot embossing (Photograph courtesy of CSEM)

bonding or lamination can be used to seal microchannels. These processes have in common that they are fast, with typical processing times of less than 10 min. They are typically performed at temperatures around 100°C, depending on the softening point of the polymers employed. Substrate materials for hot embossing or injection molding include polycarbonate (PC), polypropylene (PP), polymethylmethacrylate (PMMA), and cyclic olefin copolymers (COCs) such as Topas®.

In contrast to machine-based molding techniques, conventional molding can be performed with a simple master comprising a surface relief, placed in a molding dish (Fig. 4.8). This approach, termed *soft lithography*, has become highly popular over the past few years, offering a rapid, flexible, and inexpensive route to the creation of microfluidic components on planar substrates [13]. Soft lithographic methods describe the molding of elastomeric polymers using master templates. Elastomeric siloxane polymers such as PDMS are

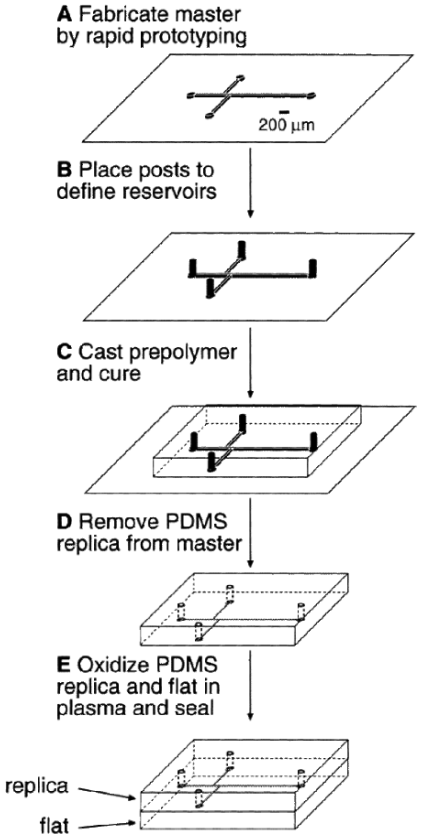

Fig. 4.8. Rapid prototyping approach for polydimethylsiloxane (PDMS) elastomer devices (Reprinted with permission from [14]. Copyright 1998 American Chemical Society)

easily molded, optically transparent (in the visible and UV regions of the electromagnetic spectrum), robust, cheap, nontoxic, and stable over wide temperature ranges. In the basic process, high aspect ratio microfluidic structures are formed by simply pouring a mixture of the elastomer precursor and a curing agent over a template. After curing, the structured polymer layer is peeled away from the template and an enclosed fluidic structure is created by contacting the elastomer with a planar surface. The seal between surfaces need not be permanent (facilitating fluidic cleaning and removal of blockages), although treatment of surfaces with an oxygen plasma allows siloxanes to be irreversibly bound to a variety of substrate materials [14].

4.2.2 Organic Semiconductor-Based Light Sources and Detectors

Lab-on-a-chip devices have shown themselves to be highly effective for laboratory-based research, where their superior analytical performance has established them as efficient tools for complex tasks in genetic sequencing, proteomics, and drug-discovery applications. However, to date they have not been well suited to *point-of-care* or *in-the-field* applications, where cost and portability are of primary concern. Although the chips themselves are cheap and small, they must generally be used in conjunction with bulky optical detectors that are needed to identify or quantify the analytes or reagents present. Furthermore, most existing detectors are limited to the analysis of a single analyte at a predetermined location on the chip. The lack of an integrated, versatile detection scheme (one which is miniaturized, integrated, wavelength-selective, and able to monitor multiple locations on the chip) is a major obstacle to the deployment of diagnostic devices in the field, and has prevented the development of more complex tests where rapid, kinetic, or multi-point analysis is required. Although there have been a few attempts to integrate optics within the chip structure itself, few have demonstrated the levels of integration demanded for *point-of-care* diagnostics.

One promising option for creating integrated light sources and photodetectors is the use of organic semiconductors. There are two main classes of organic semiconductor – the first based on small molecules [15] and the second based on polymers [16]. Broadly speaking, small molecule and polymer semiconductors have similar optical and electrical properties (although there are some notable differences) but are often processed differently. Small molecule devices are typically deposited by vacuum sublimation, which enables the controlled fabrication of complex multilayer structures but is not especially well suited to large area deposition. Polymer devices, by contrast, are typically fabricated using solution deposition techniques such as spin-coating or printing, which are better suited to large area deposition but are somewhat problematic for multilayer device fabrication (since deposition of successive layers tends to cause partial redissolution of already deposited layers).

As can be seen from Fig. 4.9, most organic semiconductor devices have simple multilayered structures, which may be fabricated in a straightforward

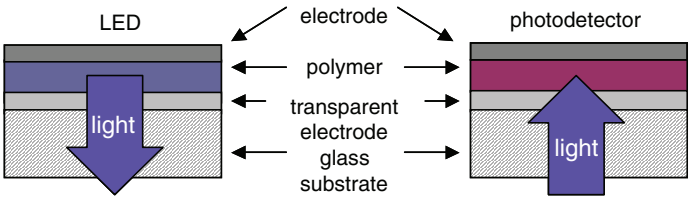

Fig. 4.9. Schematic of device structure of typical organic semiconductor-based light sources and detectors

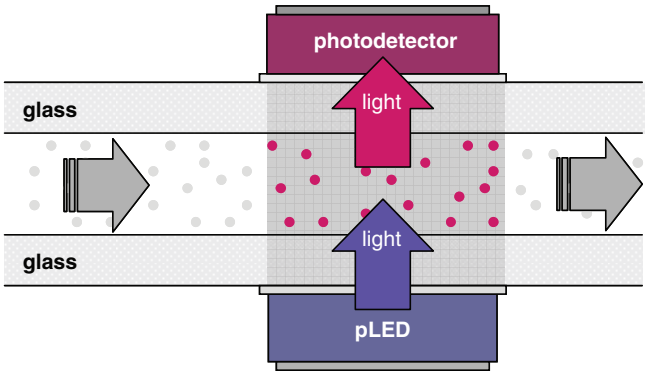

Fig. 4.10. Schematic of microfluidic detection set-up with polymer LED (pLED) light-source and organic photodetector

fashion by sequential deposition of appropriate semiconductors or electrodes. Typical thicknesses of the individual organic layers are 30–100 nm. For instance, a typical organic light-emitting diode (OLED) comprises one or more layers of semiconductor sandwiched between two electrodes, of which at least one must be transparent. The active layer emits light under electrical excitation and the devices may therefore be used as light sources. They may also be used in reverse as photodetectors by illuminating the active organic layer to generate a measurable electrical current. Accordingly, these two components may be used together as a simple detection system (Fig. 4.10). The LED and photodetector are arranged on either side (top and bottom surfaces) of a microfabricated channel containing an analyte under study. Analytes passing through the detection volume absorb photons from the OLED. Since many analytes of interest are fluorescent they may subsequently re-emit photons, which can be detected by the photodetector. Owing to the simple layer-by-layer deposition procedures for the polymer components and the planar structure of analytical microchips, such OLED/photodetector pairs may be easily integrated into existing chip structures at marginal additional cost.

There are a number of reasons why organic semiconductors are attractive as integrated sensors and some of the key advantages are discussed in Table 4.1. In short, they offer a unique means of integrating multiple light

Table 4.1. Features of organic semiconductor optics for microanalysis

Controllable properties	The properties of the LEDs and photodetectors may be systematically controlled by chemically modifying the photoactive molecules in a way that is not possible with conventional technologies. It is therefore possible to optimize light sources and photodetectors for specific analytes under investigation.
Small instrumental footprint	The active layers of organic LEDs and photodiodes are typically only a few hundred nanometers in thickness and thus add minimal weight and size to the microfluidic substrate. In most situations, the devices must be encapsulated against exposure to air and water. This can be achieved by sandwiching the organic device between substrates coated with multiple impermeable barrier layers. The inclusion of such barrier coatings only slightly increases the overall thickness of the final device, which is still significantly lower than for alternative light source and detector technologies.
Disposable use and custom fabrication	The low cost nature of organic devices and microfluidic chips make the integrated devices ideal for single-use disposable purposes, e.g., *point-of-care* applications.
Multipoint detection	As it is straightforward to fabricate arrays of closely spaced LEDs and photodetectors, it is possible to monitor the analyte at multiple locations along the flow path simultaneously. For some applications individual detectors need to be placed within 500 µm of one another to provide the spatial resolution required for useful analysis. This rules out many alternative detectors, such as photomultiplier tubes, whose physical bulk render them unsuitable for multipoint detection. Consequently, most detection methods for microanalysis have to date been limited to single-point schemes.
Solution processing and printing	In the case of polymers and solution processable molecules, high quality films may be deposited directly from solution using simple low-cost techniques such as spin-coating. This represents a major advantage over conventional semiconductors, and allows the fabrication of high-quality devices at far lower cost than using alternative technologies. The key advantage associated with soluble organic materials is the ability to use high-efficiency printing techniques (such as planographic or inkjet printing) to fabricate arrays of closely spaced OLED/photodetector pairs at precise locations on the chip substrate. The complexity of the achievable patterns is in principle limited only by the resolution of the printer, and thus enables the deposition of intricate arrays of sub-mm OLED/photodetector pairs with high precision and at low cost.

sources and photodetectors into analytical microchips without appreciably increasing the size, weight, or cost of the final device. Importantly, from the perspective of large-scale manufacturing, semiconducting polymers (and certain solution processable small molecules) are amenable to printing in much the same way as conventional inks. This offers a route for massively reducing the fabrication costs of light sources and photodetectors, and so opens up the possibility of creating disposable diagnostic devices.

The efficiencies of organic LEDs and photodetectors compare favorably with those based on conventional inorganic materials. For instance, external quantum efficiencies (defined as the ratio of photons emitted to electrons injected) as high as 29% [17] and 17% [18] have been reported for small molecule and polymer OLEDs, respectively, compared with values of 38.9% for InGaN-based devices [19]. Incident photon-to-conducted electron (IPCE) peak efficiencies of virtually 100% have been reported for both Si and organic photodiodes [20]. Importantly for sensor applications, organic photodiodes have an excellent dynamic range, and have been shown to exhibit linearity over four to six decades of light intensity (Fig. 4.11) [21].

However, there are also some respects in which organic semiconductor devices are less favorable than their inorganic counterparts. For example, it is difficult to obtain light emission below 450 nm from OLEDs and most organic photodiodes are only sensitive to light of wavelengths less than about 650 nm. The "operating window" for sensors based on pairs of organic light sources and photodetectors is therefore relatively narrow. This problem is further compounded by the broad emission from most OLEDs, which tends to span a spectral range of several hundred nanometers. The tail of the OLED emission

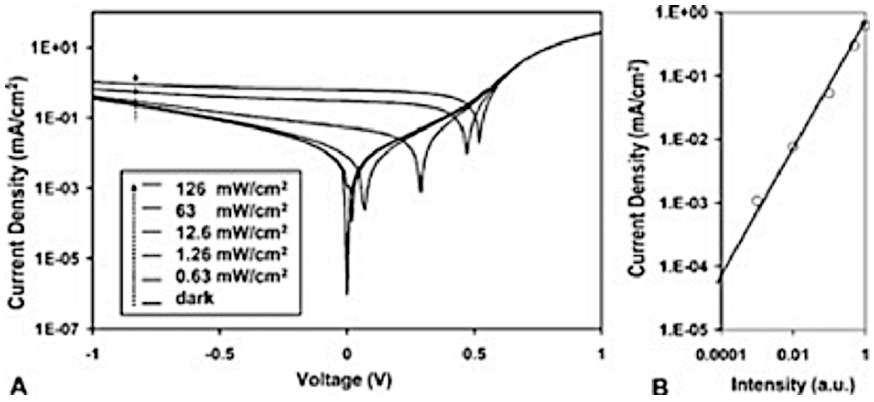

Fig. 4.11. (**a**) Current–voltage characteristics of P3HT:PCBM photodiodes under varying levels of 633 nm monochromatic illumination. See main text on pages 118 and 119 for further details about the devices. (**b**) The intensity dependence of the short-circuit photocurrent for the same device (From [21] – Reproduced by permission of The Royal Society of Chemistry)

therefore may overlap with the weaker emission from the analyte. In addition, because of the thin nature of the active layer, organic LEDs and photodiodes typically have large capacitances and so respond relatively slowly to changes in voltage or light levels, which precludes their use in certain time-resolved applications. Solutions exist to most of these issues but they introduce additional complexity into device fabrication or result in compromises elsewhere in device performance. The successful use of organic light sources and photodetectors as sensing elements is largely a question of engineering, in which one aspires to achieve sufficient detection sensitivity without making undue compromises elsewhere in the design process, e.g., cost, portability, power consumption, etc. In the following sections, we describe a number of ways in which organic light sources and photodiodes can be effectively integrated with microfluidic devices to create fully integrated self-contained sensors.

4.2.3 Towards Mass Manufacture

As noted above, semiconducting polymers (and certain solution processable small molecules) are amenable to printing in much the same way as conventional inks. There are two broad classes of printing techniques – contact methods in which the ink is physically pressed onto the surface and inkjet techniques in which the ink is squirted towards the surface. Inkjet techniques are currently the more advanced, and prototype inkjet-printed color displays as large as 40″ have been reported by companies including Sony and Samsung. Increasingly, however, attention is turning to contact-based methods such as gravure, flexographic, and offset printing, which are well suited to long print runs and historically have been applied to "low-tech" processes such as printing rolls of wallpaper. In gravure printing, for example, a recessed image is etched onto the surface of a rotating metal drum and the etched regions are filled with ink; excess ink is removed by a doctor blade and the remaining ink is transferred to a flexible film as it passes between the drum and a second roller (see Fig. 4.12). One of the key advantages of using printing techniques is the ability to switch from batch processing to *reel-to-reel* processing. The former approach suffers from considerable down-time due to the need to repeatedly load, set, and unload individual substrates whereas *reel-to-reel* processing is a continuous process that maximizes throughput. To exploit *reel-to-reel* processing it is necessary to use flexible substrate materials. This creates a number of difficulties from a technological perspective since indium tin oxide (the dominant transparent anode material for OLEDs) is typically deposited by thermal evaporation or sputtering at temperatures in excess of 350°C and, even when deposited at lower temperature, generally needs to be annealed in air or oxygen at those temperatures in order to achieve a suitably high conductivity. These issues, together with the tendency of ITO to crack when the substrate is flexed, have led researchers to seek alternative anode materials for flexible substrate applications (e.g., polymer–metal and polymer–fullerene composites and conducting polymers). Unfortunately, these materials have so far proved

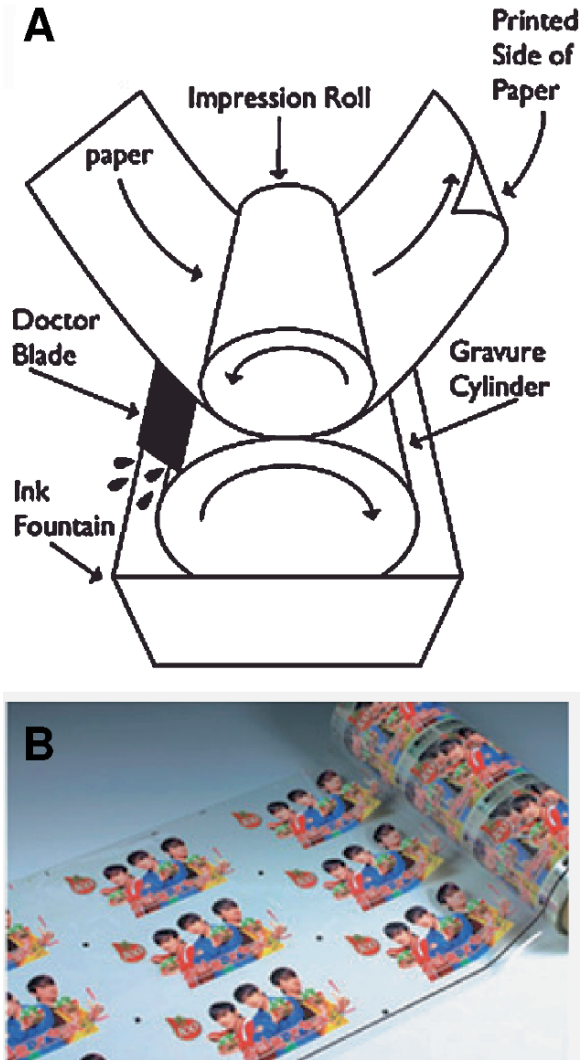

Fig. 4.12. (**a**) Gravure printing concept. (**b**) Images printed onto a flexible substrate (Pictures courtesy of Wikepedia)

inadequate for most display and lighting applications due to the difficulty of achieving a high conductivity without compromising transparency. The high sheet resistance of the resultant electrodes leads to excessive power consumption and significant heat generation, which accelerates device degradation, and considerable development is still needed before these materials are viable as electrode materials for display, lighting, and energy applications.

In the context of single-use sensors, where the devices are typically operated for just a few seconds or minutes before disposal, power consumption and

extended operating stabilities are less of an issue, and in these circumstances it is possible to dispense with ITO altogether, using instead a simple layer of a conducting polymer as the anode material. The most widely used conducting polymer for device applications is poly(3,4-dioxythiophene):polystyrenesulphonate (PEDOT:PSS) due to its reasonable transparency and conductivity and its good chemical stability in the doped state [22]. PEDOT:PSS has a much higher resistivity than ITO (at least ten times higher), but it is nevertheless possible to make light sources and photodetectors using

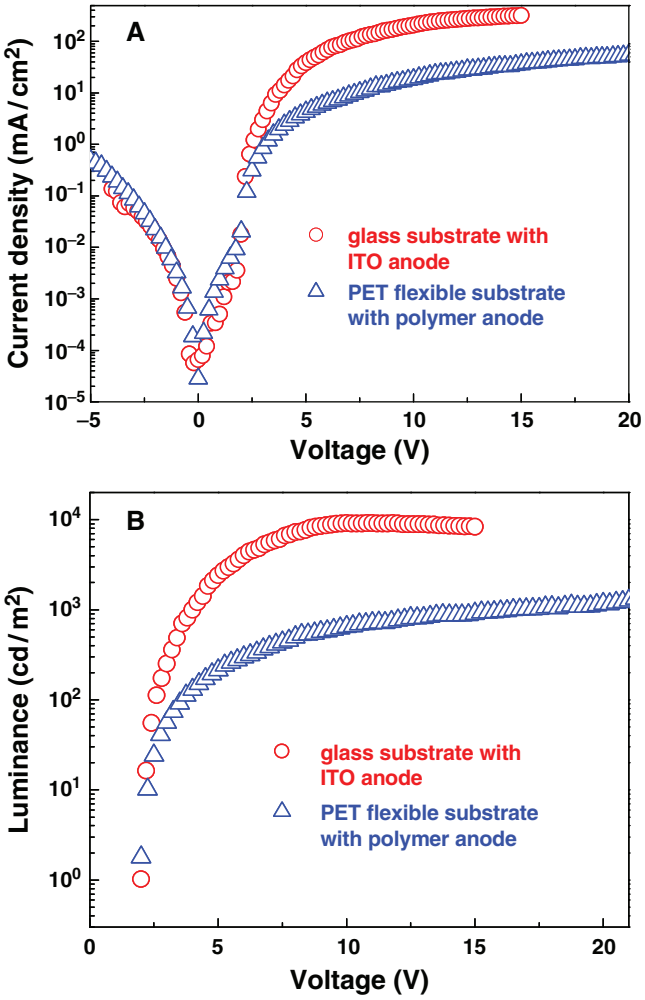

Fig. 4.13. Comparison of pLED on conventional ITO-coated glass substrate with pLED on ITO-free PET substrate. (**a**) Current density–voltage characteristics. (**b**) Luminance–voltage characteristics

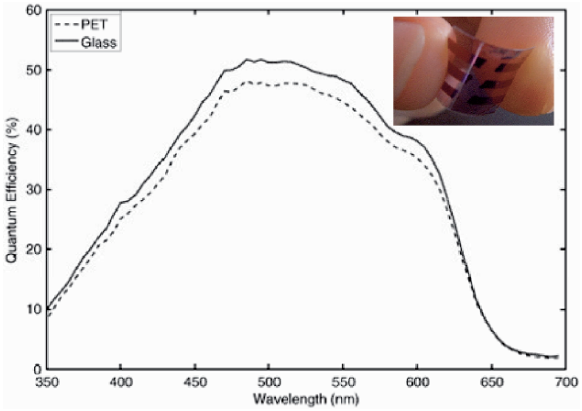

Fig. 4.14. Current–density characteristics of P3HT:PCBM photodetectors on ITO-free PET substrate. The Inset shows an image of the flexible photodetector (From [23] – Reproduced by permission of The Royal Society of Chemistry)

PEDOT:PSS anodes that are quite adequate for many sensor applications [23, 24]. In Fig. 4.13 we compare the current–voltage-luminance characteristics of a conventional LED on rigid ITO-coated glass with those of an otherwise identical device on flexible ITO-free polyethyleneterephalate (PET) coated with a PEDOT:PSS anode. The ITO free device compares reasonably well with the conventional device at moderate brightness ($<500\,\mathrm{cd\,m^{-2}}$), which is adequate for many diagnostic applications. In Fig. 4.14 we compare the spectral response of a conventional photodiode on rigid ITO-coated glass with that of an identical device on flexible ITO-free PET under (diagnostically relevant) low light levels. The quantum efficiency is virtually the same for the two devices, indicating that high quality organic photodiodes can be made on flexible substrates. It should be noted that the low conductivity of the PEDOT:PSS anode does not adversely affect the efficiency of the photodiode since the currents generated at low light levels are extremely small. The power dissipation in the anode is therefore also small and has a negligible influence on the overall efficiency of the device. At high illumination levels, as for example are incurred under solar illumination, the low conductivity of the PEDOT:PSS significantly reduces efficiencies compared with conventional ITO-containing devices. Hence, although the use of conducting polymer anodes is already more than sufficient for the diagnostic applications described in this chapter, it will be some years before they are suitable for solar energy applications.

In summary, the combination of flexible light sources and photodetectors with microfluidic chips fabricated from elastomers such as polydimethylsiloxane can enable the fabrication of low-cost all-plastic sensors that are ideally suited to low-cost *point-of-care* applications.

4.3 Functional Optical Components

In this section we describe in more detail the three key optical components for integrated fluorescence detection: (1) light sources, (2) detectors, and (3) optical filters. We also present proof-of-principle studies from our group describing the use of these components in chemical and biological analysis.

4.3.1 OLED Light Sources for Microchip Analysis

For microchip analysis, optical detection is often preferred due to the versatility and high sensitivities afforded by this technique. Although in the laboratory sophisticated benchtop mounted optics are commonly used for on-chip optical detection, this is clearly not an option for portable diagnostic applications. There exists a clear need for small low-cost optical components to replace the benchtop counterparts such as lasers, photomultiplier tubes (PMTs), or even sophisticated fluorescence microscopes. On the light source side organic light emitting diodes (OLEDs) present a viable alternative that can be integrated onto the microchip platform without significantly increasing the system complexity or power requirements. To this end we have pioneered the use of polymer light emitting diodes (pLED) as excitation sources for fluorescence detection in on-chip electrophoretic analysis (Fig. 4.15) and have also demonstrated their successful use in a diagnostic assay for kidney disease.

In our first study [25], we sought to assess whether polymer light-emitting diodes could be used as a "plug-in" replacement for mercury lamp excitation in chip-based capillary electrophoresis systems. The microfluidic device was fabricated in glass using standard lithographic techniques, and is shown

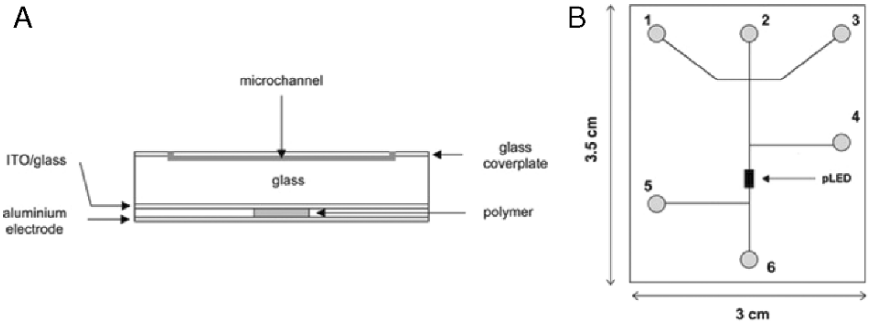

Fig. 4.15. (**a**) Side view (not to scale) of pLED integrated with a planar glass CE microdevice. (**b**) Layout of the CE microdevice comprising an injection channel and a variable length separation channel: 1, sample inlet; 2, buffer inlet; 3, sample outlet; 4–6, buffer inlets (4 and 5 unused). Microchannels are 50 µm wide and 40 µm deep. The pLED (active area: $40 \times 1{,}000\,\mu m^2$) is positioned below the separation channel between outlets 4 and 5 (From [25] – Reproduced by permission of The Royal Society of Chemistry)

schematically in Fig. 4.15a, b. Prior to the measurements, the buffer channel between ports 2 and 6 was prefilled with buffer solution. The injection channel was then filled with fluorescein solution at the sample inlet (1) by applying vacuum to the sample outlet (3), thereby displacing the buffer solution at the microchannel intersection. The sample volume in the intersection (≈100 pL) was then injected into the separation channel by application of an electric field (∼1 kV cm^{-1}) between the buffer inlet (2) and outlet reservoir (6). The arrival of the fluorophores at the pLED excitation zone was monitored using microscope optics and an external silicon diode. The pLED used for this work was a blue-emitting device based on a polyfluorene copolymer with an emission spectrum that matches well with the absorption spectrum of fluorescein (Fig. 4.16). The device was fabricated by sequentially depositing poly(3,4-ethylenedioxy-thiophene):polystyrene-sulfonate [PEDOT:PSS], 70 nm of the active layer, and a LiF/Al cathode onto an ITO-coated glass substrate. In use, signal-to-noise (S/N) ratios as high as 800 were obtained when the pLED was driven at 7 V, and separations of a variety of dye molecules including fluorescein and 5-carboxyfluorescein could easily be detected with mass detection limits of 50 fmol. The separation chip was then retested using a standard Hg lamp as the excitation source and broadly comparable results were obtained, indicating that the pLEDs can indeed be used as plug-in replacements for conventional light-sources. These studies demonstrated the first application of

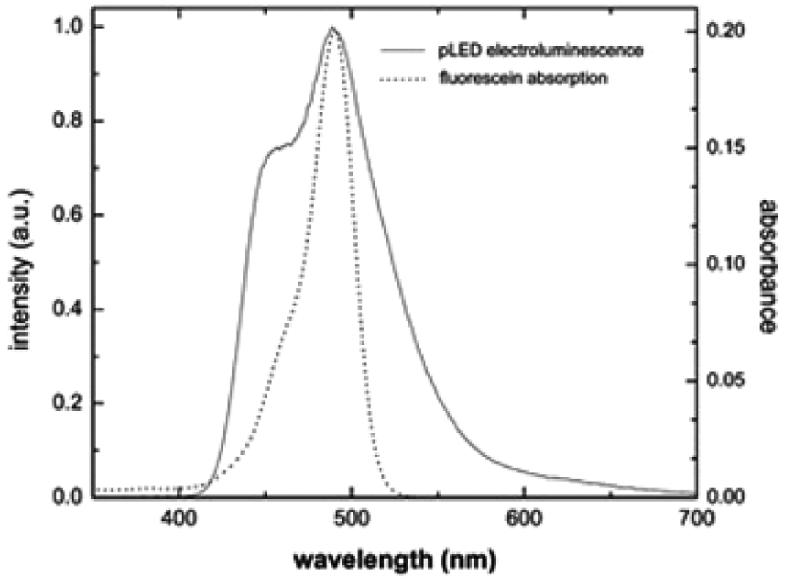

Fig. 4.16. Absorption and normalized electroluminescence emission spectra of 10 µM fluorescein and the polyfluorene pLED, respectively (From [25] – Reproduced by permission of The Royal Society of Chemistry)

thin-film polymer LEDs as integrated light sources for chemical analysis, and moreover afforded sensitivity and detection limits comparable to conventional mercury lamp excitation.

The variation of the total signal relative to the pLED signal and *S/N* as a function of the pLED applied bias is shown in Fig. 4.17a. It can be seen that at low drive voltages (4–5.5 V) an approximate linear increase in the ratio of total signal-to-pLED emission is observed. This ratio reaches a limiting value of ∼8.5 for drive voltages above 7 V. It is interesting to note that the variation of *S/N* does not follow the same trend; in fact a continuous increase in *S/N* is observed as drive voltage is increased. We attribute this trend to the significantly lower noise levels encountered at higher pLED drive voltages. While these initial calibration studies clearly indicate that for sensitive detection high pLED drive voltages are beneficial, this can also severely compromise output stability and reduce the device lifetime. Consequently, for analytical applications we decided on a compromise driving voltage of 5.5 V.

Subsequent experiments were aimed at determining the sensitivity and linear range of our pLED based detection system. Figure 4.17b shows a calibration plot for fluorescein for a pLED driving voltage of 5.5 V. A detection limit of ∼1 µM was established with a linear range spanning over four decades. These studies represent the first demonstration that pLEDs present a viable and low-cost alternative light source for high-sensitivity on-chip detection. In more recent studies we have also successfully used a poly(*p*-phenylene vinylene) (PPV) derivative OLED light source to monitor a diagnostically relevant fluorescence binding assay for renal disease. This work will be described in more detail in Sect. 4.4.1.

Current research efforts are focused on increasing the light output without compromising the lifetime of OLEDs. Further work is directed at extending the range of available OLED light sources to the red part of the light spectrum and to narrow the emission bandwidth, e.g., by using microcavity architectures.

4.3.2 Organic Photodetectors for Chemiluminescence Assays

One of the preferred methods for analyte detection in microfluidic devices is based on the phenomenon of chemiluminescence (CL), which offers a simple but sensitive means of monitoring low level analyte concentrations [26]. CL reactions typically involve the formation of a metastable reaction intermediate or product in an electronically excited state, which subsequently relaxes to the ground state with the emission of a photon. CL is particularly attractive for portable microfluidic assays, because the CL reaction acts as an internal light-source, thereby lowering instrumental requirements and significantly reducing power consumption and background interference compared to fluorescence assays. CL-based systems have been successfully applied to on-chip electrophoretic separation of metal ions, immunoassays, and enzyme assays [27], and consequently there is considerable interest in

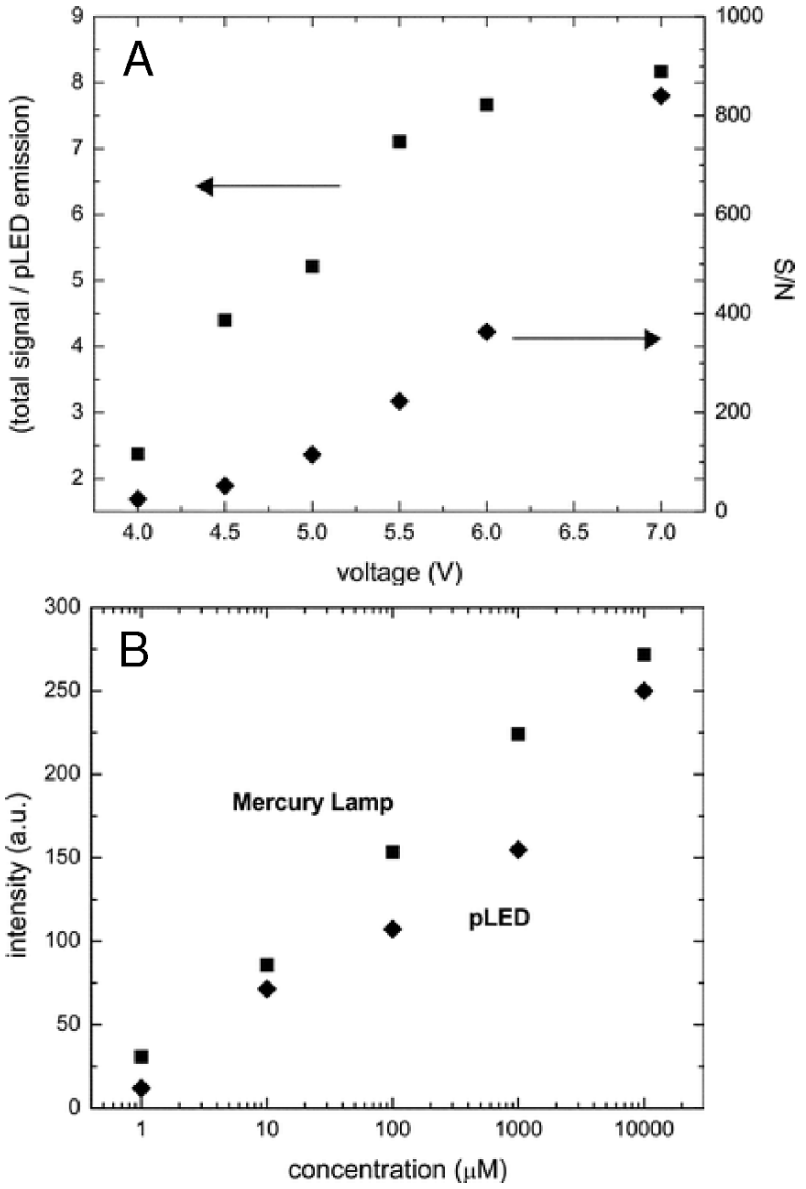

Fig. 4.17. (**a**) Variation of total signal to pLED emission ratio and signal-to-noise ratio as a function of pLED applied bias. (**b**) Calibration plot for fluorescein with on-chip mercury arc lamp and polyfluorene pLED excitation (drive voltage 5.5 V) (From [25] – Reproduced by permission of The Royal Society of Chemistry)

creating complete analytical devices that incorporate a CL assay and optical detector in a single integrated package.

In early reports of CL detection in microfluidic environments, the CL signal was generally detected and quantified using externally mounted photomultiplier tubes (PMTs) and/or microscope collection optics. Recently, however, Jorgensen et al. reported the use of integrated silicon photodiodes for monitoring peroxyoxolate-based chemiluminescence (PO-CL) reactions in micromachined silicon microfluidic chips [28]. They selected hydrogen peroxide as a model compound for quantitation, since it is produced by a number of enzymes in the presence of dissolved oxygen and certain analytes such as alcohol, glucose, and cholesterol. Using this approach they were able to attain measurable signals down to 10 µM, thus showing that high sensitivity chip-based CL detection could be implemented in a fully integrated microscale format.

The use of silicon photodiodes and micromachined silicon substrates, however, entails relatively expensive fabrication techniques that preclude the use of such devices in disposable *point-of-care* applications where low cost is of primary concern. In recent work, therefore, we investigated whether integrated microscale CL could be implemented in a lower cost format using polydimethylsiloxane (PDMS) instead of silicon as the substrate material and organic photodiodes in place of the Si detectors [28]. As previously discussed, PDMS has good biocompatibility and optical transparency over the visible range, and allows for rapid prototyping and scalable manufacturing at low cost and with high reliability. At the same time, organic devices may be fabricated at low temperature using simple layer-by-layer deposition procedures that are fully compatible with plastic substrates. The combination of PDMS microfluidic devices with organic photodiodes therefore offers an attractive route to fabricate low cost diagnostic devices, which incorporate the fluidic networks and the detectors in a single monolithic package.

In our first proof-of-principle studies, we used organic photodiodes based on vacuum-deposited bilayers of copper phthalocyanine (CuPc) and fullerene (C_{60}) to detect the emission signal from a PO-CL assay [29]. These measurements confirmed the feasibility of using organic devices for detection of the CL signal, but yielded relatively poor detection limits of 1 mM compared to 10 µM reported by Jorgensen et al. The low detection limits were attributable in part to a significant mismatch between the photodiode area ($\sim$16 mm^2) and the detection zone on the microfluidic chip ($\sim$2 mm^2), which resulted in a high background signal ($\sim$1 nA) due to the high photodiode dark current.

To improve the limit-of-detection, we replaced the 16 mm^2 vacuum deposited CuPc/C_{60} bilayer devices with 1 mm^2 solution-processed polymer devices based on 1:1 blends by weight of poly(3-hexylthiophene) [P3HT] and [6, 6]-phenyl-C61-butyric acid-methylester [PCBM] – a soluble derivative of C_{60}. The P3HT:PCBM devices fabricated in our laboratory typically have very low short-circuit dark current densities of $<10^{-6}$ mA cm^{-2}, and are consequently a good choice for high sensitivity detection [21]. The

$1 \times 1\,\mathrm{mm}^2$ dimensions of the P3HT:PCBM devices were well matched to the $800\,\mu\mathrm{m} \times 1\,\mathrm{mm}$ detection zone of the microfluidic chip and thus minimized the background signal due to the dark current. The thin-film polymer photodiodes, when integrated with PDMS microfluidic chips, provide compact, sensitive, and potentially low-cost microscale CL devices with wide-ranging applications in chemical and biological analysis and clinical diagnostics.

The microscale CL devices consist of two parts: a Y-type micromixer fabricated in PDMS and a P3HT:PCBM-based photodiode supported on a glass substrate (Fig. 4.18). The channels of the micromixer were formed in a 2 mm layer of PDMS and were sealed with a 1 mm "lid" of unstructured PDMS. Finally, fluidic access holes were punched in the 2 mm PDMS layer to enable injection and extraction of the CL reagents. The depths of all channels in the micromixer were 800 µm, while the respective widths of the inlet and mixing channels were 400 and 800 µm. The inlet channels were 1 cm long and the length of the mixing channel was 5.2 cm (Fig. 4.18a). The organic photodiode comprised a 1 mm ITO-coated glass substrate that was successively coated with (1) a 60 nm layer of poly(3,4ethylenedioxythiophene):polystyrene-sulphonate (PEDOT:PSS) [Baytron P AI 4083]; (2) a 150 nm layer of 1:1 by weight regioregular poly(3-hexylthiophene) (P3HT) and 1-(3-methoxycarbonyl)-propyl-1-phenyl-(6,6)C61 (PCBM); and (3) a 200 nm Al cathode. The $1 \times 1\,\mathrm{mm}^2$ active area of the pixel was defined by the spatial overlap of the ITO anode and the Al cathode. The entire device was encapsulated in an inert nitrogen atmosphere by securing a metal can (fitted with a desiccant patch) to the coated side of the glass substrate with a UV-cured adhesive.

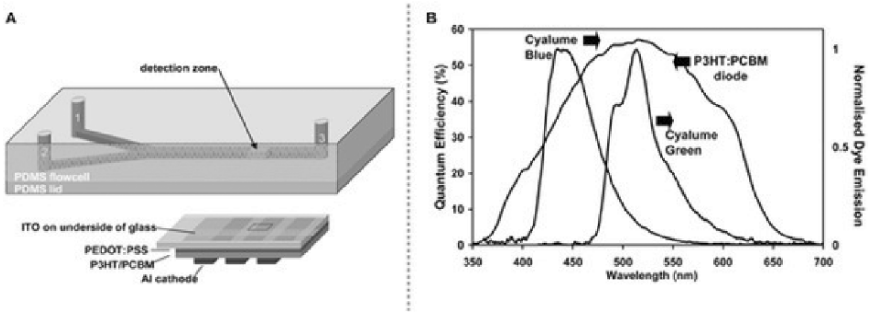

Fig. 4.18. (**a**) Schematic of PDMS microchip used for on-chip chemiluminescence assay. Reagents are loaded into inlets 1 and 2 and are hydrodynamically pumped towards outlet three. Light is generated when the two reagents mix. For detection a P3HT:PCBM photodetector is placed underneath the detection chamber of the microchip. (**b**) Responsivity of the organic photodetector and emission spectra of the chemiluminescence dyes (From [21] – Reproduced by permission of The Royal Society of Chemistry)

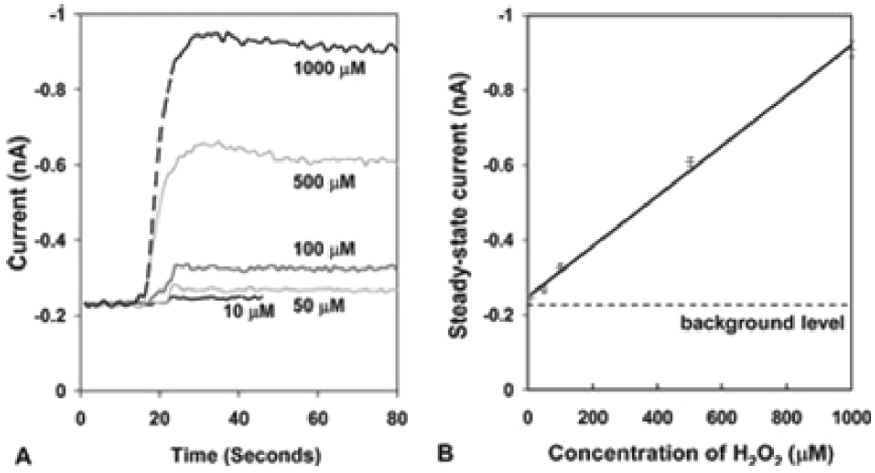

Fig. 4.19. (**a**) Transient chemiluminescence signal as recorded with P3HT:PCBM photodetector for different hydrogen peroxide concentrations (oxidation reagent). (**b**) Calibration plot for steady-state signal (From [21] – Reproduced by permission of The Royal Society of Chemistry)

The integrated CL device was completed by attaching the lid of the PDMS microchip to the glass side of the thin-film organic photodiode to form an integrated device in which the organic pixel was aligned with a detection zone on the fluidic chip and located 1 cm downstream of the point-of-confluence of the two inlet streams (see Fig. 4.18a). To perform the on-chip CL measurements, a stock solution (A) of CL reagent was first prepared by extracting the PO-CL reagents from Cyalume green light sticks (Omniglow, West Springfield, MA), which contain the active ingredients bis(2-carbopentyloxy-3,5,6-trichlorophenyl) oxalate (CPPO), dimethylaminopyridine (DMAP) catalyst, and the green dye molecule 9,10-bis(phenylethynyl)anthracene. Test solutions (B) were prepared by diluting 31% aqueous H_2O_2 stock solution with acetonitrile and adding 5 mM imidazole catalyst (Sigma-Aldrich). Additional measurements were undertaken using the Cyalume blue dye, which contains the dye molecule 9,10-diphenylanthracene. The two dyes have quantum efficiencies close to unity (0.91 ± 0.08 and 0.85 ± 0.03 for Cyalume green and Cyalume blue, respectively) and so are good choices for high sensitivity CL assays. The chemiluminescence spectra for the blue and green luminescent dyes are shown by the grey lines in Fig. 4.18b, and are essentially identical to the corresponding photoluminescence spectra for the dyes (not shown) in accordance with the indirect nature of the PO-CL emission mechanism. The emission spectra of the two dyes match reasonably well with the response of the photodiodes.

To initiate the CL reaction, the dye/catalyst mixture and the H_2O_2 were pumped hydrodynamically into inlets 1 and 2, respectively and, after waiting

an appropriate time for the signal to settle, detection was performed 1 cm downstream of the point-confluence. The steady-state CL signal is plotted against hydrogen peroxide concentration in Fig. 4.19, and excellent linearity is obtained in the range 10 µM to 1 mM. The detection limit for the integrated chip/detector was <10 µM, which represents a 100-fold improvement compared to the data obtained using the CuPc/C_{60} devices described previously. Significantly, the sensitivity of the integrated CL devices described here is equivalent to that of the devices reported by Jorgensen et al. using integrated silicon photodiodes.

The limit-of-detection for our devices is determined primarily by the background signal (dark current) of the organic photodiodes, and current studies are aimed at reducing the dark current through improved device fabrication procedures. Changes to the CL chemistry may also enable appreciable increases in emission intensity since the Cyalume dyes used are primarily optimized for emission longevity and, in the current context, a short-lived high-intensity emission is preferable. We anticipate that taken together these changes may enable a further 100- to 1,000-fold improvement in detection limits. The current 10 µM limit-of-detection is already sufficient for many diagnostic applications, including the determination of alcohol, glucose, and cholesterol levels in blood. Further improvements to the 100 nM level will provide sufficient sensitivity for applications such as low level cancer marker detection and pharmacokinetics.

Finally, we note that these initial studies were conducted in a lab environment using standard instrumentation and equipment that is ill-suited to miniaturized low-cost applications. In ongoing studies, we are evaluating the use of on-chip reagent storage methods and passive capillarity-based fluid delivery schemes that remove the need for external fluid motivation. Such devices would offer a powerful low cost solution for chemical and biological analysis with potentially wide-ranging applications for *in-the-field* analysis and *point-of-care* diagnostics.

4.3.3 Optical Filters for Head-On Fluorescence Detection

In conventional fluorescence detection, the excitation source and detector are usually arranged orthogonally to one another to prevent direct illumination of the detector by the excitation source. This orthogonal geometry, however, is difficult to implement in a microfluidic environment since it requires the integration of optical components onto the side-surfaces of the microfluidic chip. Light sources and detectors are most conveniently located on the upper and lower faces of the microfluidic chip in a colinear geometry, but this often leads to detector saturation, with direct light from the excitation source masking the weaker fluorescence from the analyte. The key to achieving effective discrimination of the excitation and emission light in this "head-on" configuration is the use of a long-pass filter in front of the detector to block the excitation light and transmit the longer wavelength emission signal. The use of long-pass

filters for this purpose is well established but has generally involved the use of discrete stand-alone filters – an approach that yields satisfactory optical performance but prevents monolithic integration and leads to inefficient collection of the fluorescence signal.

In this respect, it is preferable to use optical filters that are monolithically integrated with both the photodetector and the microfluidic chip substrate. Surprisingly, only a few monolithic approaches have been reported in the literature. One successful example was reported by Burns et al. who described the use of integrated filters in silicon-based microfluidic devices. In their work multilayer interference filters were fabricated on top of PIN silicon photodiodes [30]. The interference filters typically comprised up to 40 alternating layers of SiO_2/TiO_2 with ∼5%-transmittance at 490 nm and ∼90%-transmittance at 510 nm, and resulted in significant performance gains when incorporated into DNA analysis chips. An alternative lower cost approach was recently reported by Chediak et al., who developed integrated color filters for silicon microfluidic devices using thin layers of cadmium sulphide deposited directly on top of PIN silicon photodiodes [31]. The CdS filters exhibited strong blocking of the excitation light but relatively low transmission of the emission light (∼40%). In addition thin-film CdS is known to exhibit appreciable fluorescence so, although not discussed by the authors, it is likely that these filters would exhibit significant autofluorescence – a serious issue for on-chip detection as discussed later.

The interference-filters and CdS-filters described above could in principle be straightforwardly integrated with glass microfluidic chips, but they are unsuitable for conformable elastomeric materials such as PDMS – a preferred substrate material for low-cost disposable applications – since polycrystalline materials such as CdS, TiO_2, and SiO_2 are typically deposited at relatively high temperatures (>300°C) and have a tendency to crack when the substrate is flexed.

All the above approaches also introduce additional steps of varying complexity into the fabrication process and, from a technological perspective, a preferable solution would be to use the microfluidic substrate itself as the color filter. The simplest way to implement this is to disperse appropriate dye molecules into the substrate material (plastic or glass) prior to chip fabrication. The colored substrate thereby obtained is able to serve concurrently as the microfluidic medium and optical filter, negating the need for an additional filter layer and allowing for improved collection of the fluorescence since the detector can be placed in closer proximity to the channel (Fig. 4.20). The dispersal of dye molecules in polymer matrices to produce color filters is well established, but the successful utilization of this approach to produce a dual-functioning microfluidic chip and color-filter presents a number of challenges: (1) the colinear detection geometry and typically weak intensity of the analyte emission necessitate a sharp filter cut-on with excellent blocking and transmission on either side; (2) because of the close proximity of the filter and photodetector, filter autofluorescence must be negligible

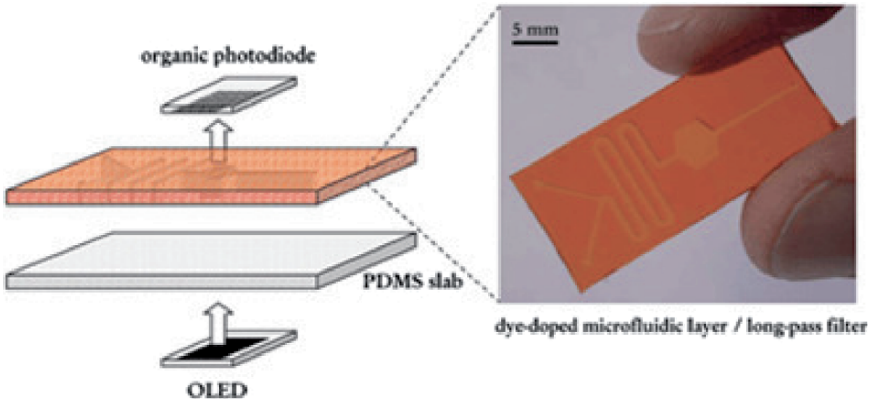

Fig. 4.20. Illustration of monolithically integrated optical filter concept. The dye-doped PDMS substrate serves concurrently as microfluidic conduit and optical longpass filter (From [32] – Reproduced by permission of The Royal Society of Chemistry)

since it is liable to raise the background signal from the photodiode and thus mask the analyte signal; (3) the incorporation of dye molecules into the host matrix must conserve the processability of the polymer, enabling high quality microfluidic chips to be fabricated from the dye-doped polymer; and (4) the resultant colored substrates must be stable (on the timescale of the experiment) against dye leaching due to solvent flow through the channel and photodegradation. The fabrication of high quality integrated microchip filters that retain the excellent processability of standard undoped PDMS but have comparable optical characteristics to state-of-the-art commercial filters is therefore a genuine challenge. Fortunately, we have found that the dispersion of lysochrome dyes into PDMS substrates offers a particularly effective solution (Fig. 4.21). In our method lysochrome dyes are dissolved in a small volume of apolar solvent and added to the PDMS monomer prior to polymerization over a master comprising the microfluidic layout. The resultant filters have excellent optical characteristics, e.g., red long-pass filters with $<0.01\%$ transmission at 500 nm and $>80\%$ transmission above 570 nm, which compares favorably with commercially available Schott glass filters. Importantly, such filters showed negligible autofluorescence, allowing them to be effectively employed in microchip-based fluorescence detection [32]. The filters proved robust in use, undergoing negligible leaching in aqueous solution and only marginal photodegradation under prolonged exposure to UV light. Patterning of the PDMS was unaffected by the dye doping, allowing for the fabrication of colored substrates that serve concurrently as channel medium and optical filter. In initial work, we were primarily interested in developing a range of long-pass filters. However, for diagnostic applications involving organic light-emitting diodes, short-pass filters are also of considerable importance. This is because organic semiconductors are broad-band fluorophores that typically

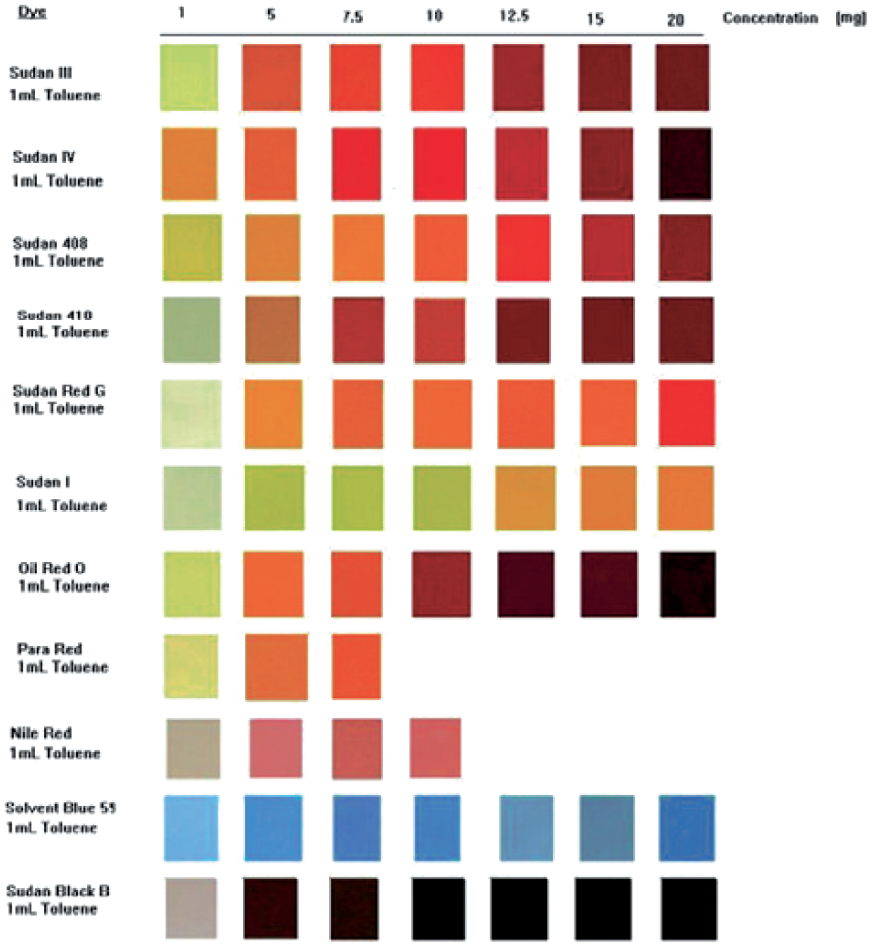

Fig. 4.21. Overview of available shortpass, longpass, and blocking filter based on dye-doping of the PDMS microfluidic substrate

have a long emission tail that extends several hundred of nanometers beyond the peak emission wavelength. This long tail tends to overlap and mask the analyte emission. To avoid this problem, short-pass filters are required between the LED and the channel to sharpen the emission from the LEDs and allow analyte emission to be detected. We have developed a broad range of short and long-pass filters for diagnostic applications, a selection of which can be seen in Fig. 4.21.

4.4 Applications

In this section we describe how the functional components described above have been applied to real-world analytical applications.

4.4.1 Microalbuminuria Determination On-Chip

As a first application for our integrated microfluidic platforms with organic semiconductor-based components we investigated the determination of microalbuminuria (MAU) in urine. MAU is defined as an increased urinary excretion of human serum albumin (HSA), which is indicative of renal problems in diabetic patients [33]. The American Diabetes Association thus recommends an annual MAU test for all diabetic patients to monitor the success of the diabetes treatment. Furthermore, MAU has recently been recognized as a potential risk factor for cardiac disease and is also known as an effective marker for battlefield trauma associated with blast damage. When MAU is detected at an early stage reno-protective and antihypertensive treatment can be applied to prolong patient's lives. Although semi-quantitative MAU dipstick tests are available for *point-of-care* use, unambiguous diagnosis can only be achieved through subsequent lab-based quantitative tests with sophisticated readers. Accordingly, the aim of our research was to enable quantitative MAU analysis at the *point-of-care* by developing a microfluidic chip-based analysis platform (with integrated OLED based detection) that could be used in the doctor's surgery or for home-testing by the patient itself.

An effective fluorescence binding assay originally developed by Kessler and coworkers was selected as a suitable assay format [34]. The assay is based on the Albumin Blue 580 (AB580) dye, which binds specifically to HSA, resulting in an enhancement in the fluorescence emission of two orders of magnitude. From a microfluidic point of view, MAU determination in urine is inherently simple in that no sample pretreatment is required (unlike blood-based diagnostics that often require sample filtration), with only two components being mixed during the assay (the albumin containing sample and AB580). From a detection point of view, conditions are also favorable in that there is a low background signal (AB580 on its own is only very weakly fluorescent) while the emission from the AB580-HSA complex is comparatively strong. Furthermore, the clinically relevant cut-off concentration for MAU of 15–40 mg L^{-1} HSA is high compared to other diagnostic markers such as Troponin, Myoglobin, and CK-MB in blood (typical cut-off limits <10 µg L^{-1}).

To achieve effective mixing of the sample and probe solutions we used a simple PDMS microfluidic device [35]. The device comprises two inlets, a meandering mixing channel, a widened detection chamber, and an outlet. The inlets were 400 µm wide, 800 µm deep, and 1 cm long, while the mixing channel was 800 µm wide, 800 µm deep, and 5.2 cm long (Fig. 4.22). The extended trapezoidal detection chamber was 5 mm long, 5 mm wide, and 1.6 mm deep. The total internal volume of the microchip was ~27 µL. For initial testing we used standard syringe pumps to drive the HSA and AB580 solutions through the microchannel network. In our latest devices, however, as described in Sect. 4.4.3 we are using passive filling schemes. Optical excitation in the detection chamber was achieved through the use of a yellow thin-film OLED based on a light emitting poly(*p*-phenylene vinylene) (PPV) derivative. The device

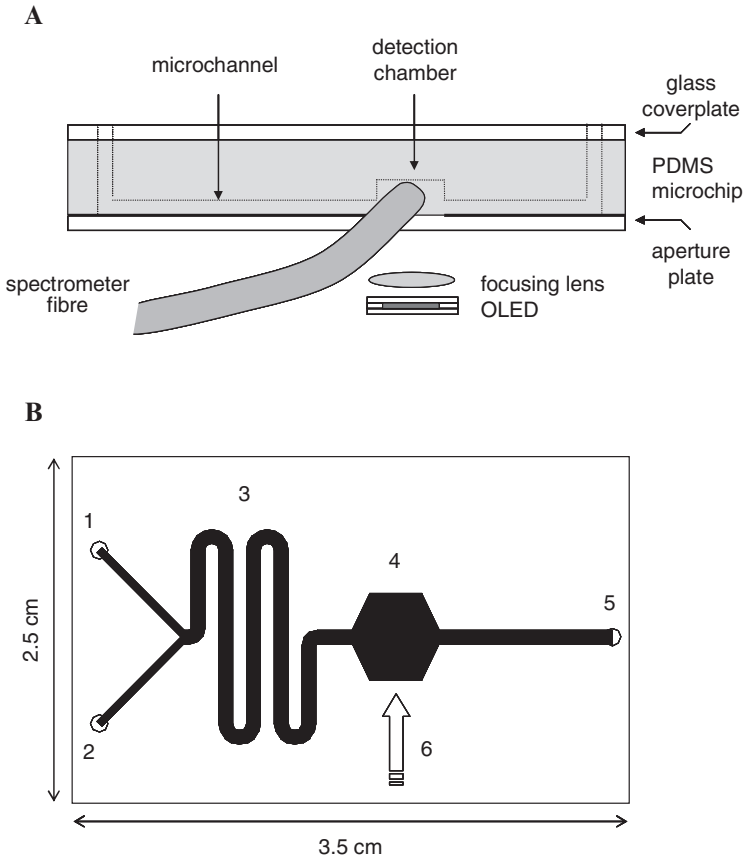

Fig. 4.22. (**a**) Schematic of experimental set-up for microalbuminuria determination. (**b**) Microchip layout with inlets for AB 580 (1) and HSA (2), mixing channel (3), detection chamber (4), outlet (5), and orthogonal detection point (6) (From [35] – Reproduced by permission of The Royal Society of Chemistry)

structure comprises a patterned indium tin oxide (ITO)-coated glass substrate, a hole-injecting layer of poly(3,4-ethlenedioxythiophene):polystyrenesulfonate (PEDOT:PSS), the active PPV emission layer, and a thermally evaporated cathode layer with a lithium fluoride layer capped with aluminum. A metal encapsulation can comprising a desiccant patch was sealed against the glass substrate using epoxy adhesive.

Figure 4.23 shows the yellow OLED emission that spans from 500–700 nm with a maximum at 540 nm. As can be seen, the emission overlaps appreciably with the absorption spectrum of the HSA/AB580 complex rendering the OLED an efficient excitation source for this application. Emission from the HSA/AB580 complex spanned from ∼580–700 nm with a maximum at 610 nm. In a standard collinear "head-on" detection geometry with OLED

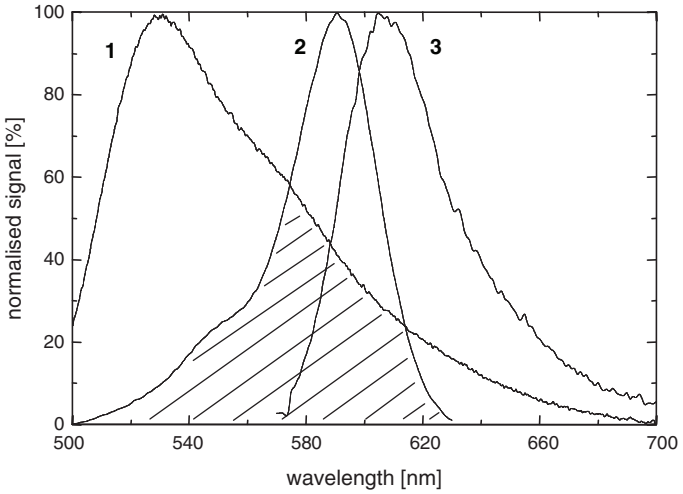

Fig. 4.23. OLED emission spectrum (1) and overlap with excitation (2) and emission spectra (3) of 1.2 µM AB 580 dye after addition of 100 mg L^{-1} HSA (From [35] – Reproduced by permission of The Royal Society of Chemistry)

and detector on either side of the microchannel, this overlap of complex emission with the tail of the OLED emission would necessitate optical filtering (e.g., the use of a short-pass filter on the light source side to cut off the tail of the OLED emission). The work described here predated our development of integrated short-pass and long-pass filters as described in Sect. 4.3.3. Hence, to circumvent this requirement we implemented an orthogonal detection geometry with the OLED light source positioned below the microfluidic chip and detection performed from the side, thereby minimizing the amount of OLED light hitting the detector.

To excite the HSA/AB580 complex on-chip, the yellow OLED was typically driven at 20–30 mA (7–8 V bias), yielding a brightness of 8,000–10,000 cd m^{-2}. To detect the complex emission a CCD spectrometer fiber was brought in close contact with the side surface of the microchip adjacent to the detection chamber. Initial results revealed an unusually high amount of detected excitation light, presumably due to light scatter of the diverging OLED light at the sidewalls of the detection chamber. The OLED contribution was greatly reduced through the use of an aperture between the OLED and the microchip, with the aperture size matched to the detection chamber. Typical complex spectra for HSA concentrations in the range 1–1,000 mg L^{-1} are depicted in Fig. 4.24a. To compensate for potential OLED intensity variations, the spectra were normalized to the 550 nm light source band. A general increase of the HSA/AB580 emission band at 620 nm can be observed for HSA concentrations above 10 mg L^{-1} with the pure AB580 dye serving as a negative control.

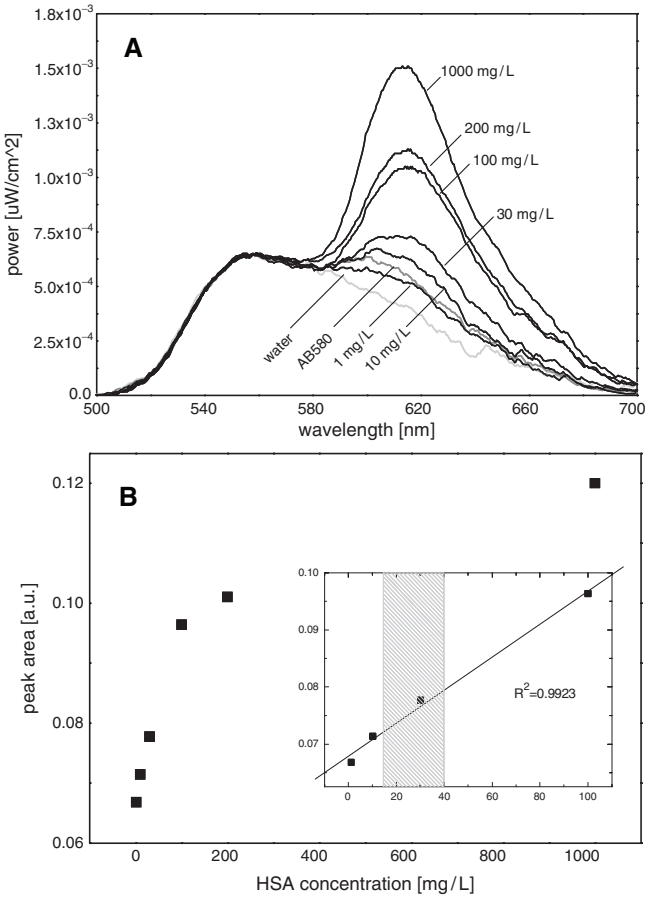

Fig. 4.24. Detection of different HSA concentrations after mixing with 1.2 µM AB 580 dye. (**a**) Spectra normalized on 550 nm peak. (**b**) HSA quantitation via peak area 500–700 nm. Inset shows linear range in diagnostically relevant HSA concentration range. Hatched area corresponds to 15–40 mg L^{-1} cut-off limit for MAU (From [35] – Reproduced by permission of The Royal Society of Chemistry)

Quantitation was subsequently performed by integration of the light intensity between 500 and 700 nm. The resulting calibration plot of peak area vs. HSA concentration is depicted in Fig. 4.24b. Although a strong signal increase is observed for lower HSA concentrations, the signal plateaus at very high concentrations due to the excess of AB580, which is consistent with previously published data. More importantly linearity between 1–100 mg L^{-1} HSA is obtained with an estimated limit-of-detection (LOD) of <10 mg L^{-1}. This is sufficient for the determination of MAU in a clinical setting with typical cut-off levels of 15–40 mg L^{-1} and compares to LODs of approximately 2 mg L^{-1} for cuvette-based measurements on conventional benchtop fluorometers.

While the successful application of OLED excitation sources for chip-based MAU determination clearly represents an important step towards the realization of portable diagnostic tests, engineering challenges still remain, especially the need to replace the expensive CCD with a low cost organic photodetector. To this end we are currently implementing organic photodetector to replace the employed CCD camera. This is most conveniently achieved in a colinear format rather than the orthogonal geometry employed here. To this end we are currently working on the integration of a short-pass filter on the OLED side (to cut off the emission tail) and long-pass filters on the detector side (to cut-off the OLED light while transmitting the longer wavelength analyte emission). As described in Sect. 4.4.3 we are also working on the implementation of passive microchip filling schemes to circumvent the use of bulky pumps for reagent delivery.

4.4.2 Chemiluminescence-Based Diagnostic Tests

As noted previously, CL offers a simple but sensitive means of monitoring low level marker concentrations in a microfluidic format. CL is particularly attractive for portable microfluidic assays because the CL reaction acts as an internal light source, thereby lowering instrumental requirements and significantly reducing power consumption while at the same time providing low background interference [36]. CL reactions typically involve the formation of a metastable product in an electronically excited state, which subsequently relaxes to the ground-state with the emission of light (direct CL). Indirect CL methods also exist where an electronically excited reaction intermediate is formed, followed by energy transfer to an emitting receptor dye. The most commonly used indirect method is PO-CL, where an oxalate ester is oxidized by hydrogen peroxide, resulting in the formation of metastable C_2O_4 and energy transfer to a variety of receptor dyes such as diphenylanthracene (blue), 9,10-Bis(phenylethynyl)anthracene (green), rubrene (yellow), rhodamine 6G (orange), and rhodamine B (red). The commercial availability of the reagents and the broad range of available emission colors render the PO-CL assay an ideal test platform for our chip-based portable diagnostic tests.

Potential analytes for PO-CL assays include oxidants, CL enhancers/quenchers, and fluorophore labels (e.g., the dyes listed above linked to a detection antibody, which is specific to the targeted marker). In chip-based diagnostic CL assays, however, specificity is most commonly afforded by upstream enzymatic assays that generate hydrogen peroxide only in the presence of a specific analyte (e.g., alcohol, glucose, and cholesterol) and dissolved oxygen. The generated hydrogen peroxide can then be detected through the generation of light when mixed with the peroxyoxalate reagent and a reporter dye. As discussed in Sect. 4.3.2, for our initial proof-of-concept tests we mixed varying concentrations of hydrogen peroxide with the PO-CL reagent and a green dye and recorded the resulting CL emission with our P3HT/PCBM

organic photodetectors. We observed a linear dynamic range from 10 µM to 1 mM and a limit of detection <10 µM hydrogen peroxide, which is already sufficient for many diagnostic applications such as the determination of alcohol, glucose, and cholesterol in blood. However, further improvements to sub-100 nM levels are required to provide sufficient sensitivity for low-level cancer marker detection and pharmacokinetic applications.

For the first diagnostic application of our organic photodiode-based CL system we selected the determination of antioxidant capacity [37]. Antioxidants, either as food additives or as pharmaceutical supplements can terminate radical reactions in vivo, which can otherwise damage essential molecules such as nucleic acids and proteins. In a healthy person the production of reactive oxygen species (ROS) is balanced by the antioxidant defense system. However, in "oxidative stress" situations a serious imbalance between the production of ROS and antioxidant defense can occur. In such cases the intake of antioxidant is essential to prevent cell damage. The PO-CL assay described above provides a straightforward means of assessing the effectiveness of different antioxidants. In our initial experiments, antioxidant standards are injected into a hydrogen peroxide stream, which is subsequently reacted with the PO-CL reagent and an acceptor dye. The antioxidant standard essentially scavenges the hydrogen peroxide and hence reduces the CL emission that is generated.

Figure 4.25a depicts the recorded signal from the organic photodiode in response to the injection of varying concentrations of the known antioxidant Vitamin E [38]. As expected a decrease of CL emission is observed for the injection of each plug, which increases for higher antioxidant concentrations. Interestingly, some positive signal deviation before and after plug injection is also observed, which we assign to laminar flow-based stacking effects. Figure 4.25b shows similar signal profiles for unknown plant-based antioxidant extracts. Again a signal decrease is observed and an antioxidant content value can be calculated. The same experiment was repeated with conventional PMT-based detection and the comparison of the results is displayed in Fig. 4.26. It can be seen that the results are in good agreement, yielding a ranking order of the examined plant extracts.

While we have demonstrated the successful application of our integrated organic photodiode-based test platform to antioxidant capacity determination, we regard this as a first step towards a universal platform for chemiluminescence-based testing at the *point-of-care*. To this end we have investigated the use of passive fluid delivery schemes (to circumvent the use of valves and external pumps) and the implementation of low-cost electronic read-out circuits (for both size and cost reduction).

Figure 4.27 depicts a first demonstration system that comprises a microfluidic chip, an organic photodiode, and a low-cost printed circuit board (PCB) with amplifier. Powering and read-out is performed through a handheld computer. Future battery-driven devices are also envisaged to comprise an

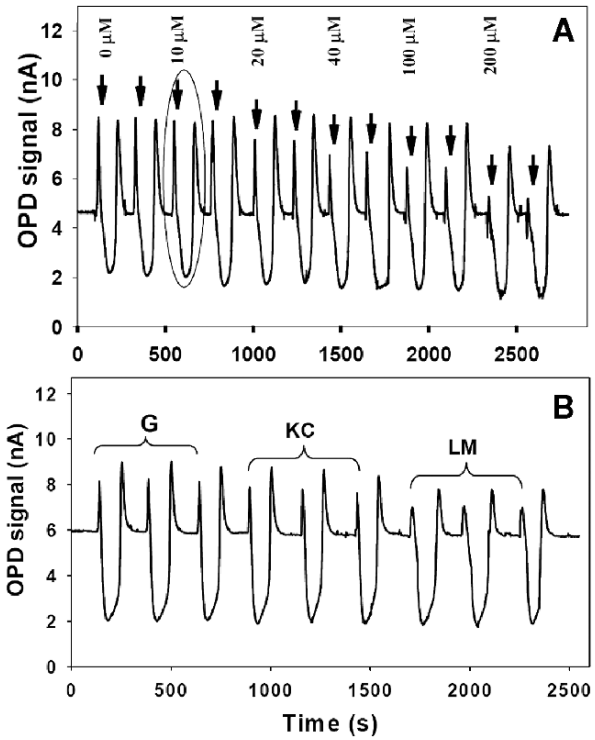

Fig. 4.25. PO-CL signal profiles after (**a**) duplicate injections of Vitamin E standards and (b) sequential injection of untested plant extracts Alpinia galanga – G, Kaempferia galanga – KC, and Cymbopogon citratus – LM (**b**) (From [37] – Copyright 2007 Springer)

integrated data display. In the current device assays are initiated by applying 30 µL of PO-CL reagent/dye and hydrogen peroxide, respectively, into the two inlet ports of the microchip. Filling of the microfluidic circuit is initiated by removing a lid from the microchip outlet, resulting in pressure equilibration and capillarity-driven filling of the microchannels. Diffusional mixing of the two reagent streams then occurs across the laminar flow interface. By the time the two reagent streams reach the detection chamber, which is positioned on top of the organic photodiode, the entire fluidic contents would have intermixed, resulting in CL emission. After closing the demonstrator lid, the photocurrent of the organic photodiode can be measured and subsequently quantitated against hydrogen peroxide concentration. Using this low-cost and passive technology, we have been able to achieve detection limits similar to our lab-based systems using syringe pumps and sensitive electrometer instrumentation.

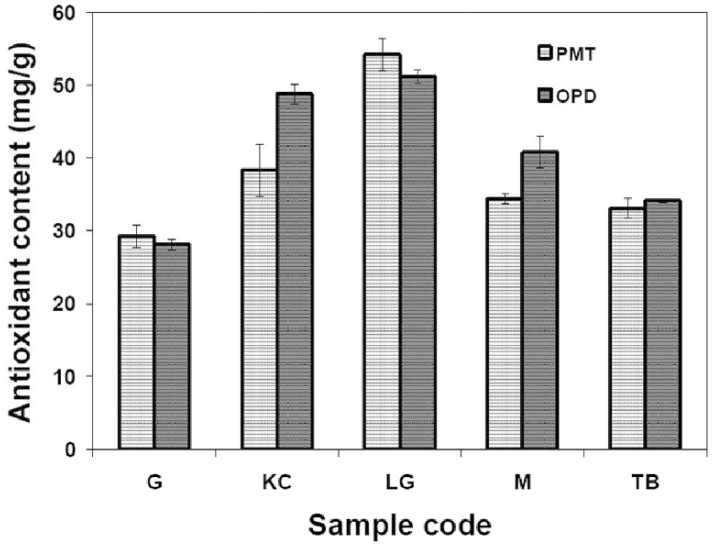

Fig. 4.26. Comparison of estimated antioxidant content of five herbal extracts as measured with P3HT:PCBM photodetector and PMT. G, Alpinia galanga; KC, Kaempferia galanga; LM, Cymbopogon citratus; M, Mentha piperita; TB, Ocimum spp (From [37] – Copyright 2007 Springer)

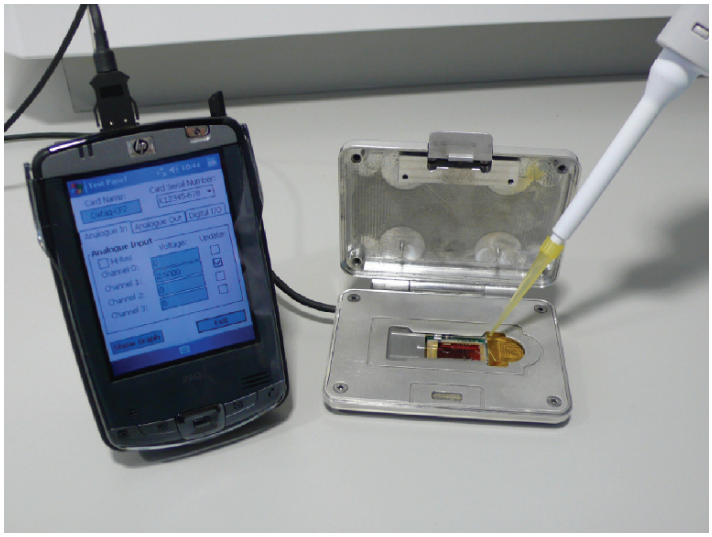

Fig. 4.27. Picture of chemiluminescence demonstrator with integrated organic photodiode and low-cost electronics

4.4.3 Towards Portable and Disposable Diagnostic Devices

Although the last two decades have seen significant breakthroughs in microfluidic technology, commercial success has been somewhat elusive. The few microfluidic-based analytical systems that have penetrated the market are primarily based on cartridge-reader systems where the microfluidic functionality is integrated in a disposable cartridge while read-out and data acquisition is accomplished in dedicated and often costly benchtop-sized reader systems. A typical example is Agilent's Bioanalyzer^{TM} system, which offers a variety of cartridges aimed at DNA sizing, and protein and cell binding assays (Fig. 4.28). Such benchtop-sized microfluidic devices have proven to be very powerful, e.g., DNA sizing can be accomplished in a few minutes compared to several hours or even days using standard gel electrophoresis techniques. However, there are significant drawbacks in that such systems remain bulky, require training or skilled staff, and their high cost is often prohibitive for use in the home or developing countries. The maturation of organic semiconductor-based detection technology provides a viable route towards the adaptation of powerful benchtop-sized microfluidic systems into portable, autonomous devices that can ultimately be made low-cost and disposable. When targeting the *in-the-field* or *point-of-care* diagnostic markets, additional design considerations have to be addressed [39]. First, there is a need for a user-friendly interface that allows simple sample application of the required bodily fluid. Sophisticated sample pretreatment methods as commonly used in clinical laboratories (e.g., centrifugation) are clearly not an

Fig. 4.28. Bench-top Agilent 2100 Bioanalyzer^{TM} with fluidic cartridge (Photograph courtesy of Agilent Technologies)

option for *point-of-care* use [40]. While urine samples can be directly assayed within microfluidic device, whole blood samples often require a filtration step to prevent blood cells from obstructing the microfluidic circuit [41]. Fortunately there exist a variety of methods for on-chip blood filtration, such as the use of microfabricated pillar arrays with pitches smaller than the diameter of blood cells. Secondly, once applied the sample should ideally be processed autonomously without requiring any further user intervention. This can be conveniently achieved using capillarity-based passive fluid delivery schemes, which circumvent the use of bulky pumps. Here, sample processing, such as the mixing with stored on-chip reagents, can be controlled via careful design of the microfluidic circuit. Read-out of the generated assay signal can then be achieved through integrated organic semiconductor-based detection systems with inherently low power requirements. For stand-alone devices (e.g., for home testing) low power requirements are essential in order to enable battery driven operation, but more sophisticated devices could draw power from widely available electronic consumer products such as mobile phones or PDAs. The main advantages of such configurations stem from the enhanced data processing power and added data handling capabilities, which for instance could enable wireless connections to a general practitioner (for test result evaluation) or connection to medical databases for data storage.

To this end we have developed an organic semiconductor based fluorescence demonstrator for *point-of-care* diagnostic testing (Fig. 4.29). The fluorescence demonstrator comprises an OLED-based light source in the lid, which is

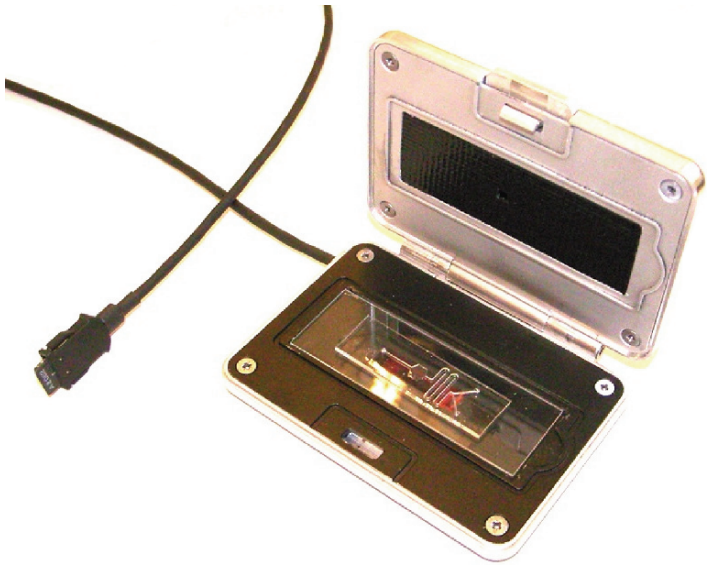

Fig. 4.29. Picture of fluorescence demonstrator with OLED light source (*in lid*), integrated organic photodetector (*in base*) and low-cost electronics

controlled via an integrated printed circuit board (PCB). The base of the demonstrator comprises an organic photodetector with integrated filtering and read-out electronics. A microfluidic chip is placed on top of the organic photodetector such that the detection chamber coincides with the detector pixel used for measuring the signal. After loading the sample into one of the two inlet ports of the microfluidic chip, a strip is removed from the outlet port to initiate autonomous filling and on-chip fluidic processing. When the lid of the device is in the closed position, the OLED light source is located on top of both the detection chamber and organic photodetector, resulting in a head-on or co-linear configuration. This allows for excitation of sample contained in the microfluidic detection chamber and measurement of any emitted fluorescence. To prevent excitation light from saturating the detector and thereby masking any analyte emission, optical filtering is required. In the described device an integrated optical long-pass filter is thus employed on the detector side to effectively block the light source contribution while transmitting the longer wavelength analyte fluorescence. Using fluorescent nanospheres as labels we can currently perform analyte detection in the nanomolar concentration range, and are working on lowering detection limits down to the picomolar range in order to widen the range of diagnostic assays that can be implemented in our low-cost detection platforms.

4.5 Conclusions and Outlook

The success of microfluidic systems as basic experimental tools in chemistry and biology has in large part been driven by a range of fundamental features that accompany system miniaturization. As has been shown, such features include the ability to process and handle small volumes of fluid, large improvements in analytical performance when compared to macroscale systems, reduced instrumental footprints, low unit cost, and facile integration of functional components. The last decade has seen a truly astonishing amount of research activity in the field of microfluidics. Significantly, the theoretical predictions (of increased efficiencies, speeds, throughput, and control) have in general been borne out by experiment, and integrated microfluidic systems are now being successfully used to solve a number of fundamental problems that have been inaccessible using conventional analytical instrumentation. Despite the obvious fact that functional integration of analytical components can be used to create microdevices that are physically small, the primary motivation for their development has been to perform chemistry and biology in a faster, more efficient, and more controlled fashion. Indeed, many early predictions of credit card-sized devices capable of performing complex analytical processes have been slow to materialize. As discussed, the lack of highly integrated microfluidic devices applicable to POC diagnostics has in large part been defined by the difficulties associated with integrating detectors that are small, sensitive, rapid, cheap, and applicable to the analysis of a wide range of biological analytes.

Fortunately, the technologies described in this chapter have begun to fulfill the above requirements and suggest a bright future for microfluidic-based POC diagnostics. Very simply, detectors based around organic semiconductors can in principle be mass-manufactured at extremely low unit cost using established processing methods, provide for sensitive optical detection in a range of formats and importantly can be tailored to fit many fluorescence-based biological assays. All these features are required for the mass deployment of POC diagnostic systems in a variety of environments. Although any POC diagnostic system will exhibit the core characteristics described previously, the application environment will dictate further specific qualities that must be realized. For example, a microfluidic POC diagnostic test for pathogen detection in Sub-Saharan Africa needs to be rugged, low-cost, suitable for operation by an unskilled user, have a long shelf-lifetime, be able to process samples containing contaminants and/or particulates, and operate within wide temperature and humidity regimes. On the other hand a microfluidic POC device for the detection of myocardial infarction by first responders in the US needs to provide a fast *time-to-test* result, but does not necessarily need to operate within wide temperature ranges or be able to function in dirty environments. Consequently, the acceptance, introduction, and sustainability of microfluidic POC diagnostic devices will ultimately be defined by the ability to lower unit costs to a level that is competitive with current test formats (such as lateral flow assays) while significantly improving performance markers (such a time-to-test result, accuracy, and quality control). This is by no means a simple task and commercial inertia in accepting these new formats is likely to be significant.

A number of key advances must be accomplished in the short-to-medium term if integrated microfluidic systems are to become established in the POC market. First, all the functional components within the device (i.e., microfluidic circuitry, detectors, and control circuitry) need to be fabricated using an integrated and continuous process to allow mass fabrication at low unit cost. Second, it is expected that most reagents required for a particular assay will be stored (in a solid form) on-chip and activated at the time of use. Accordingly, a key focus of future studies will address reagent capture, storage, and release procedures within microfluidic circuits. In a similar fashion, for many applications (e.g., in developing countries) it is expected that microfluidic POC devices may be stored for extended periods of time before use. Thus novel encapsulation approaches will need to be developed to ensure long shelf-lifetimes for both polymer LED and photodetector elements. Other areas of research focus will include the integration of multiple tests on single chip devices (panel testing) and the integration of components for data management and transferal to data bases.

In conclusion, it is clear that microfluidic formats offer immense, potentially revolutionary opportunities for POC diagnostics. Although in its infancy, the field of microfluidic technology has demonstrated a remarkable capability for analyzing, manipulating, and processing minute amounts of biological fluid. Nevertheless, the establishment and acceptance of robust *lab-on-a-chip*

devices in medical diagnostics is still an aspiration, but one we hope will become a reality within the next five years.

References

1. A.J. deMello, Nature **442**, 394 (2006)
2. D.R. Reyes, D. Iossifidis, P.A. Auroux, A. Manz, Anal. Chem. **74**, 2623 (2002)
3. P.A. Auroux, D. Iossifidis, D.R. Reyes, A. Manz, Anal. Chem. **74**, 2637 (2002)
4. S.C. Terry, J.H. Jerman, J.B. Angell, IEEE Trans. Electron Devices **26**, 1880 (1979)
5. D.J. Harrison, K. Fluri, K. Seiler, Z.H. Fan, C.S. Effenhauser, A. Manz, Science **261**, 895 (1993)
6. R.G. Blazej, P. Kumaresan, R.A. Mathies, Proc. Natl. Acad. Sci. USA **103**, 7240 (2006)
7. P. Yager, T. Edwards, E. Fu, K. Helton, K. Nelson, M.R. Tam, B.H. Weigl, Nature **442**, 412 (2006)
8. A.J. de Mello, Lab Chip **3**, 29N (2003)
9. E. Verpoorte, Lab Chip **3**, 42N (2003)
10. K.B. Mogensen, H. Klank, J.P. Kutter, Electrophoresis **25**, 3498 (2004)
11. M.J. Madou, *Fundamentals in Microfabrication: The Science of Minaturization*, 2nd ed. (CRC Press, Boca Raton, 2002)
12. H. Becker, L.E. Locascio, Talanta **56**, 267 (2002)
13. J.C. McDonald, D.C. Duffy, J.R. Anderson, D.T. Chiu, H.K. Wu, O.J.A. Schueller, G.M. Whitesides, Electrophoresis **21**, 27 (2000)
14. D.C. Duffy, J.C. McDonald, O.J.A. Schueller, G.M. Whitesides, Anal. Chem. **70**, 4974 (1998)
15. T.U. Kampen, *Low Molecular Weight Organic Semiconductors* (Wiley-VCH, Weinheim, 2007)
16. G. Hadziioannou, G.G. Malliaras, *Semiconducting Polymers: Chemistry, Physics and Engineering*, 2nd ed. (Wiley-VCH, Weinheim, 2007)
17. D. Tanaka, H. Sasabe, Y.J. Li, S.J. Su, T. Takeda, J. Kido, Jpn. J. Appl. Phys. Part 2: Lett. Express Lett. **46**, L10 (2007)
18. Weblink (2007) http://www.japancorp.net/Article.Asp?Art_ID=14153
19. M.C. Schmidt, K.C. Kim, H. Sato, N. Fellows, H. Masui, S. Nakamura, S.P. DenBaars, J.S. Speck, Jpn. J. Appl. Phys. Part 2: Lett. Express Lett. **46**, L126 (2007)
20. J. Drechsel, B. Mannig, F. Kozlowski, D. Gebeyehu, A. Werner, M. Koch, K. Leo, M. Pfeiffer, Thin Solid Films **451–452**, 515 (2004)
21. X.H. Wang, O. Hofmann, R. Das, E.M. Barrett, A.J. Demello, J.C. Demello, D.D.C. Bradley, Lab Chip **7**, 58 (2007)
22. J. Huang, P.F. Miller, J.S. Wilson, A.J. de Mello, J.C. de Mello, D.D.C. Bradley, Adv. Funct. Mater. **15**, 290 (2005)
23. J. Huang, X. Wang, X.Y. Kim, A.J. deMello, D.D.C. Bradley, J.C. deMello, Phys. Chem. Chem. Phys. **8**, 3904 (2006)
24. J. Huang, R. Xia, Y. Kim, X. Wang, J. Dane, O. Hofmann, A. Mosley, A.J. de Mello, J.C. de Mello, D.D.C. Bradley, J. Mater. Chem. **17**, 1043 (2007)
25. J.B. Edel, N.P. Beard, O. Hofmann, J.C. deMello, D.D.C. Bradley, A.J. deMello, Lab Chip **4**, 136 (2004)

26. P. Fletcher, K.N. Andrew, A.C. Calokerinos, S. Forbes, P.J. Worsfold, Luminescence **16**, 1 (2001)
27. Z.Y. Zhang, S.C. Zhang, X.R. Zhang, Anal. Chim. Acta **541**, 37 (2005)
28. A.M. Jorgensen, K.B. Mogensen, J.P. Kutter, O. Geschke, Sens. Actuators B Chem. **90**, 15 (2003)
29. O. Hofmann, P. Miller, P. Sullivan, T.S. Jones, J.C. deMello, D.D.C. Bradley, A.J. deMello, Sens. Actuators B Chem. **106**, 878 (2005)
30. M.A. Burns, B.N. Johnson, S.N. Brahmasandra, K. Handique, J.R. Webster, M. Krishnan, T.S. Sammarco, P.M. Man, D. Jones, D. Heldsinger, C.H. Mastrangelo, D.T. Burke, Science **282**, 484 (1998)
31. J.A. Chediak, Z.S. Luo, J.G. Seo, N. Cheung, L.P. Lee, T.D. Sands, Sens. Actuators A Phys. **111**, 1 (2004)
32. O. Hofmann, X. Wang, J.C. deMello, D.D.C. Bradley, A.J. deMello, Lab Chip **6**, 981 (2006)
33. C.E. Mogensen, *Microalbuminuria, A Marker for Organ Damage* (London Science Press, London, 1993)
34. M.A. Kessler, A. Meinitzer, W. Petek, O.S. Wolfbeis, Clin. Chem. **43**, 996 (1997)
35. O. Hofmann, X. Wang, J.C. deMello, D.D.C. Bradley, A.J. deMello, Lab Chip **5**, 863 (2005)
36. X.R. Zhang, W.R.G. Baeyens, A.M. Garcia-Campana, J. Ouyang, Trends Anal. Chem. **18**, 384 (1999)
37. M. Amatatongchai, O. Hofmann, D. Nacapricha, O. Chailapakul, A.J. deMello, Anal. Bioanal. Chem. **387**, 277 (2007)
38. X. Wang, M. Amatatongchai, D. Nacapricha, O. Hofmann, J.C. deMello, A.J. deMello, D.D.C. Bradley, Lab Chip (submitted)
39. A.J. Tudos, G.A.J. Besselink, R.B.M. Schasfoort, Lab Chip **1**, 83 (2001)
40. C.D. Chin, V. Linder, S.K. Sia, Lab Chip **7**, 41 (2007)
41. E. Verpoorte, Electrophoresis **23**, 677 (2002)